INAS/GAAS HETEROEPITAXY: REAL-TIME REFLECTANCE-ANISOTROPY SPECTROSCOPY

M.I. ABRIL ARMENTA FRANCO

A THESIS SUBMITTED IN PARTIAL FULFILLMENT OF THE REQUIREMENTS TO OBTAIN THE DEGREE OF DOCTORATE IN APPLIED SCIENCES

DR. ALFONSO LASTRAS MARTÍNEZ

UNIVERSIDAD AUTÓNOMA DE SAN LUIS POTOSÍ

UNIVERSIDAD AUTÓNOMA DE SAN LUIS POTOSÍ
http://www.iico.uaslp.mx
2018, May

ABSTRACT

Reflectance Difference Spectroscopy (RDS) is an in-situ and in real-time measurement technique used to study optical anisotropies during InAs/GaAs(001) growth. Studies were performed in a Molecular Beam Epitaxy (MBE) ultra-high vaccum chamber under different As overpressures and several substrate temperatures. Reflectance Difference Spectroscopy was used to acquire the experimental data, which were measured with an acquisition time of 100 ms. As a mathematical tool, Singular Value Decomposition (SVD) was used to analyse the measured spectra in order to obtain representative bases $S_i(E)$ which with a linear combination of them, each of the spectra (S(E,t)) is reproduced. $S(E,t)=\sum_1^i c_i(t)S_i(E)$ is the mathematical representation of the fittings for each experimental measured data. Physical Models such as Strain are used to fit the obtained representative bases.

INTRODUCTION

This work presents a Refance Difference Spectroscopy *in-situ* and in real-time study of InAs/-GaAs(001) growth motivated by the increasing applications of this heterostructure in some technological devices as QDs lasers, qubits (for its use in quantum computers), InAs or InGaAs solar cells, etc. Such studies were performed in an MBE ultra-high vaccum chamber, under different growth conditions, i.e., different temperatures and diverse As overpressures. One of the main motivations for performing this study was to comprehend the evolution of this heteroepitaxial growth under different circumstances and to be able to apply that knowledge during the fabrication of technological devices.

For this purpose, InAs thin films were deposited in different monolayers ranges which comprises from 2 ML to 8 ML. Two different substrate temperatures were used during this study, T_1=480°C and T_2=460°C, meanwhile the As overpressure was maintained constant with a value of P=5x10^{-6}Torr. Also, a different study was made by inverting the variables where three different As overpressures were used; P_1=5x10^{-6}Torr, P_2=2x10^{-6}Torr, and P_3=6x10^{-7}Torr while a constant substrate temperature of T=480°C was maintained. Reflectance difference spectroscopy was used to analyze the growths in real-time. This technique allowed to measure the change in the anistropies as the InAs deposition went on. Two different kind of optic-electronic arrangements were used for this purpose. The first of them, consisted in a multiplexer-1-channel lock-in arrangement allowing spectra to be measured in a time range of 1 spectrum per .333 s, and the second RD spectrometer was conformed by a 32-channel lock-in with a 32-channel phototube arrangement, allowing the time rate to reduce to 1 spectrum per .1 s, as well as the noise to diminish notoriously. The description of these two different spectrometer arrangements as well as the MBE vaccum chamber and RHEED characterization technique is done in **Chapter 1** of this work.

On the other hand, **Chapter 2** consists on the description of GaAs and InAs most studied reconstructions, as well as the results obtained by other studies with different characterization techniques during the deposition of InAs/GaAs(001). Also, a small description of a mathematical resource used during the analyses of the RDS spectra, Singular Value Decomposition (SVD) is done in this chapter.

Last but not less important (actually the core of this work), a description of the evolution of each of the experiments is done in **Chapter 3**. This chapter is divided by the measurements made by the different spectrometers and is subdivided by the different physical characteristics of each experiment. In each of the cases, RDS spectral components (described in Chapter 2) as well as its corresponding coefficients are presented. Not surprisingly, a well known lineshape can be seen in each of the spectral components, the strain lineshape. As it is well known from other studies, due to the lattice mismatch of these cubic semiconductors, an orthorrombic strain is developed during the growth, allowing it to be released as InGaAs islands, reason why each of the spectral components have this characteristic RDS strain form. Besides, a fitting to the measured spectra done by the least square method, is also presented in this chapter. As a complement, diffraction patterns showing the reconstruction evolution in time and RHEED oscillations were measured during the growth.

In this work, RDS is consolidated as a strong and fine characterization technique during heteroepitaxial growth, being able to detect every single change in the cubic structure of these semiconductors during growth, as it is a time-resolved spectroscopy.

CONTENTS

1 EXPERIMENTAL BACKGROUND 1
1.1 Introduction 1
1.2 Molecular Beam Epitaxy (MBE) 1
1.3 Reflection High-Energy Electron Diffraction (RHEED) 2
1.4 Real-Time Reflectance Difference Spectroscopy (RDS) 5
1.4.1 **RDS Experimental Setup** 5

2 THEORETICAL BACKGROUND 9
2.1 Introduction 9
2.2 Semiconductors Growth Mode 9
2.3 GaAs(001) Surface Reconstructions 11
2.3.1 **GaAs(001) c(4x4) and (2x4) Surface Reconstructions** 11
2.4 Characterization of InAs/GaAs(001) Growth 14
2.4.1 **Studies of InAs Quantum Dot Growth** 14
2.4.1.1 **InAs/GaAs(001) RD Spectra Characterization** 14
2.4.1.2 **InAs QD's/GaAs STM Surface Reconstruction Characterization** 15
2.4.1.3 **InAs QD's /GaAs(001) AFM and RHEED Height and Density Characterizations** 20
2.5 Singular Value Decomposition and RDS Spectra 22
2.5.1 **SVD applied to Real-Time RDS spectra** 22
2.6 Reconstruction-Induced Strain and RDS Spectra 26
2.6.1 **Linear Model** 27

3 EXPERIMENTAL RESULTS 31
3.1 InAs Sample and Experimental Setup Preparation 31
3.2 Heteroepitaxial Growth; RDS measurements with a 32-channel Lock-In 31
3.2.1 **InAs/GaAs(001) growth at T=480°C** 32
3.2.1.1 **RDS and RHEED measurements along** [110] 32
3.2.1.2 **RDS and RHEED measurements along** $[1\bar{1}0]$ 36
3.2.2 **InAs/GaAs(001) growth at T=460°C** 40
3.2.2.1 **RDS and RHEED measurements along** [110] 40
3.2.2.2 **RDS and RHEED measurements along** $[1\bar{1}0]$ 44
3.2.3 **Defining S_1 and S_2 as strain bases** 48
3.3 Heteroepitaxial Growth; RDS measurements with a 2-channel Lock-In 49
3.3.1 **InAs/GaAs(001) growth at T=480°C and different As Overpressures** 49
3.3.1.1 **Measurements along** [110] **and at** $P_{As} = 5x10^{-6}$**Torr** 50
3.3.1.2 **Measurements along** [110] **and at** $P_{As} = 2x10^{-6}$**Torr** 52
3.3.1.3 **Measurements along** [110] **and at** $P_{As} = 6x10^{-7}$**Torr** 54

Appendices 61

A APPENDIX A 63
A.1 Singular Value Decomposition 63
A.1.1 Example of Full Singular Value Decomposition 63
B APPENDIX B 69
B.1 Singular Value Decomposition Wolfram Mathematica Code 69
B.2 Strain Model Wolfram Mathematica Code 70
BIBLIOGRAPHY 77

1 EXPERIMENTAL BACKGROUND

This chapter introduces the basic notions of the experimental arrangement used during the characterization of heteroepitaxial growth by means of molecular beam expitaxy (MBE). It presents its fundamental ideas as well as its distinctive features.

1.1 INTRODUCTION

The diverse applications of semiconductor devices demand the existance of experimental techniques that could assure a crystaline growth over a clean substrate with a small defect density; so, their electronic and optical properties can be preserved. The existence and utility of such epitaxial growth techniques come since 1963, with the application of liquid phase epitaxy (LPE) for the fabrication of p-n GaAs unions by H. Nelson. The main difference between the growth tecniques is defined by the transportation of the material from the source towards the substrate. Such growth techniques can be divided into three groups, a) liquid phase epitaxy, where the transportation mean is a solute saturated by the material to be deposited, then there is b) vapor phase epitaxy which takes place when diverse materials in its gaseous phase make a chemical reaction between them and with the substrate and finally c) molecular beam epitaxy where a beam of molecules of the material to be grown arise from a high-temperature effussion cell and impinge over the substrate allowing, the molecules to be adsorbed in the surface of the substrate [1]. The latter one is used during the heteroepitaxial growth in which is focused this investigation. MBE was chosen as it is easier to have a precise growth control due to its ultra-high vaccum ambient (UHV) and at the same time facilitates the usage of non-invasive characterization techniques [2] such as reflection high-energy electron diffraction technique (RHEED) and reflectance difference spectroscopy (RDS). Such measurement techniques allowed to study *in situ* and in real-time the processes which governed the crystal growth. The subsequent sections are focused in the description of these characterization techniques.

1.2 MOLECULAR BEAM EPITAXY (MBE)

As was stated before, one of the most important conditions on crystal growth is a clean substrate with a stable surface configuration and little defect density to start with. This condition ensures an epitaxial growth to take place and the optical and electronic properties of the semicondcutor to remain or be enhanced due to the growth control. This is sufficed by growing the sample under UHV conditions, which means pressures around 10^{-11} Torr [3].

The technique consists on impinging the substrate with the material in the form of molecular beams while it is contained in an UHV chamber. A molecular beam is created by heating the source material until it vaporizes while being in a cell with a tiny orifice, such cell is known

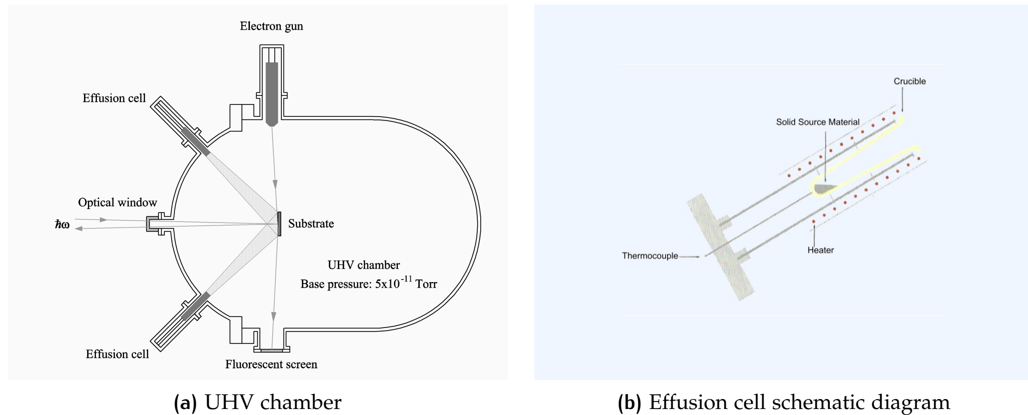

(a) UHV chamber

(b) Effusion cell schematic diagram

Figure 1: Schematic description of a MBE chamber and its effusion cell. Figures taken from ref. [1]. In a) the composition of the UHV chamber is shown by the effussion cells, the RHEED electron gun and an quartz optical window for the RDS setup. In b) the inside of one of the effussion cells is described by showing hos the solid material turns into vapor by the augmentation of the temperature in the heater.

as effusion cell and it is shown in Fig 1a and 1b , as well as the UHV chamber mentioned above. As the vapor escapes from the cell through a small nozzle, their molecules form a well-collimated beam that impinges the substrate with certain pressure, since the UHV environment outside the cell allows the escaping molecules to travel ballistically for meters without collisions. The growth is controlled by the substrate temperature, as well as the effusion cell's temperature Fig 1b. Also, the material flux is switched on and off by shutters positioned in front of the crucibles, which are actuated by computer-controlled motors. Typically several effusion cells are used at the same time, so several molecular beams impinge at unison over the substrate, allowing a film to grow epitaxially. Hence, that is from where **Molecular Beam Epitaxy** technique takes its name.

1.3 REFLECTION HIGH-ENERGY ELECTRON DIFFRACTION (RHEED)

The first time electron diffraction technique was experimentally demonstrated was in 1927 by Davisson and Germer. As once Thomson stated in the preface of 1936 "Electron Diffraction" monograph, *"... its applications provide one of the most promising lines of approach to the study of surfaces, of molecular structures and of crystal growth"*[4].

As its name states it, RHEED operates in a high energy range that is around 1 keV and 30 keV. And due to the need of the electrons to travel big distances, it works properly in a UHV environment so the electrons wont collide with any gas molecules.

The basics of the system functionality consists on a glancing incident electron beam emerging from an electron gun over the substrate with a very small incident angle and then being diffracted by the substrate's superficial atoms towards a photoluminiscence screen where its

diffraction pattern is observed, as it can be seen in Fig. 2a. When constructive interference occurs, the scattering amplitude is at its maximum value. Constructive interference occurs when the scattering vector $\Delta\vec{k}$ equals a lattice vector $\vec{G}$:

$$\vec{\Delta k} = \vec{k}_i - \vec{k}_o = \vec{G} \tag{1.1}$$

Constructive interference occurs any time a lattice point of the reciprocal lattice's surface intersects a sphere of radius k, see at Fig. 2b the so called *Ewald sphere*.

RHEED is well known for in situ monitoring of the layer by layer growth, as well as the surface structure, steps and ordering studies. The monitoring of the changes of intensity of the specular reflection beam is measured as a function of the surface's coverage. A complete layer takes place when the oscillating lineshape of the intensity reaches a maximum continuing then to the next maximum, as it's seen in Fig. 2c. This peak intensity and the valley intensity correspond to the completion of one layer and a half-filled layer, respectively. In consequence, the time between two adjacent peaks is considered to be the time that takes to a complete monolayer of the material to be deposited, therefore, the deposition rate can be calculated. It has to be taken into account that if the surface of the substrate is not smooth during the growth, then a complete oscillation is never reached and the technique cannot be used to monitor the growth rate, however, it continues to be useful as the diffraction pattern still changes with the growth, whereas it is a layer by layer growth or not. RHEED is a useful technique to monitor the deposition rate as well as the change in a growth mode, from a 2D surface to a 3D one, as it is seen during the growth of InAs quantum dots, which will be described in detail in the next sections.

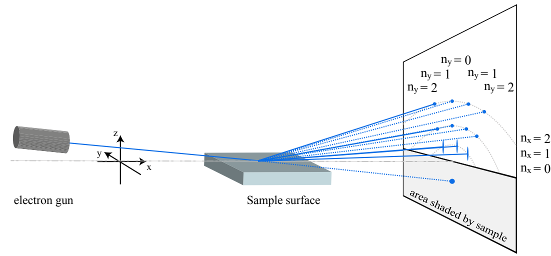

(a) Schematic diagram of RHEED's functionality

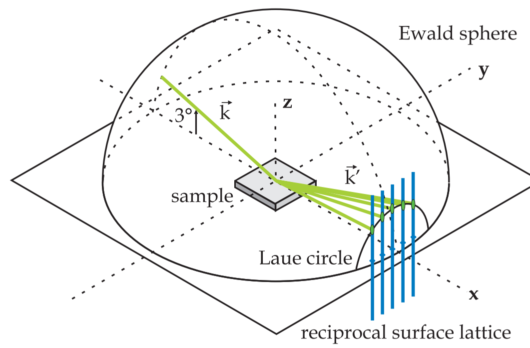

(b) Constructive interference and the Ewald sphere

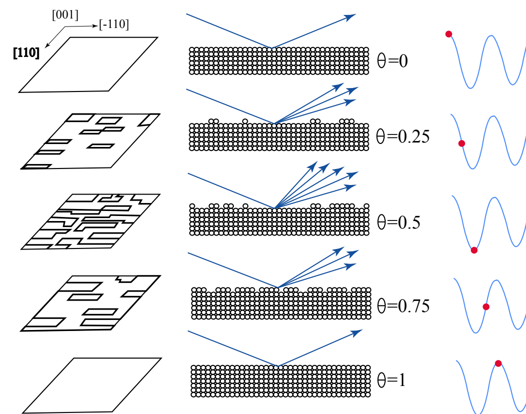

(c) Correspondance between the sample's coverage and RHEED oscillations

Figure 2: Description of RHEED monitoring tecnique, figures a) and b) were taken from reference [5] and figure c) from [6] .

1.4 REAL-TIME REFLECTANCE DIFFERENCE SPECTROSCOPY (RDS)

Reflectance modulated spectroscopies have demonstrated to be powerful techniques to characterize the optical properties of crystal semiconductors with cubic symmetry [7]. In particular, RDS is an adequate technique to measure optical anisotropies in crystals with cubic symmetry. The need of monitoring and controlling the changes a semiconductor surface experiences during growth, was a stimulus for the development of the rapid reflection anisotropy spectrometer of 16-channel described by reference [8]. However, given the need to expand the spectral range as well as the rate of data acquisition (sub-second time resolution), a 32-channel RD spectrometer was developed in 2012 by the research group of IICO, at Universidad Autónoma de San Luis Potosí [9]. In 2015, such RD spectrometer was upgraded allowing the data acquisition rate to diminish til 100 ms per spectra and augmentating the signal-to-noise ratio [10]. The latter two spectrometers are used during this research and its results are well described in the last chapter of this work.

The optical anisotropies in a cubic semiconductor are measured by taking the difference between the reflectivity (ΔR_j, j=1,2) of a pair of orthogonal crystallographic axes and normalize it to the Reflectivity [11]. Such anisotropies are originated by the brake of symmetry at the crystal's surface [12]. As the bulk symmetry remains unchanged it does not contribute to the RD spectra. Then, the reflectance difference is defined by:

$$\frac{\Delta R}{R} = 2\frac{R_1 - R_2}{R_1 + R_2} \tag{1.2}$$

where R_1 and R_2 are the corresponding reflectivities of the substrate along its two perpendicular optical axes, at normal incidence.

1.4.1 RDS Experimental Setup

The basic optical arrangement used during the experiments is described in this subsection. The RD spectrometer is mounted over an aluminum board, which is aligned at 45° relative to the floor (the horizontal), this configuration allows measurements to be simultaneous with RHEED ones. Such a spectrometer is set in such a way that the polarized incident light beam reaches the substrate along the [100] crystallographic direction allowing it to be modulated between the perpedicular crystallographic directions, [110] and $[1\bar{1}0]$, it also reaches the substrate with an angle near to normal so that the $\vec{s}$ and $\vec{p}$ light components are symmetric. The light source in this arrangement comes from a Xenon arc lamp of 75 W (USHIO, model UXL—75XE), a pair of concave mirrors guide the light beam towards a Glan-Thompson polarizer prism. Then, linearly polarized light enters the growth chamber through a fused-quartz window [13] and impinges normal to the substrate in growth. The substrate is alligned with the use of RHEED, until one of the diffraction patterns seen along directions [110] or $[1\bar{1}0]$ is shown in the photoluminiscent screen, thereby it is ensured that the polarization vector is along the crystallographic direction [100].

After the light is reflected by the substrate's surface, it leaves the growth chamber towards a 50kHz photoelastic modulator (Hinds Instruments, PEM 80). The effects of the modulator on a linear polarized monochromatic light wave are; if the optical element is relaxed, then the

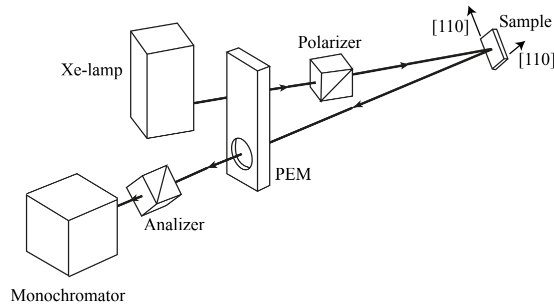

Figure 3: Experimental setup of the RD spectrometer.

light passes through with the polarization unchanged, if the optical element is compressed, the polarization component parallel to the modulator axis travels slightly faster than the vertical component. The horizontal component then "leads" the vertical component after light passes through the modulator. If the optical element is stretched, the horizontal component "lags" behind the vertical component [14]. The phase difference between the components at any instant of time is called the retardation and it corresponds to the signal that is used as reference for the lock-in.

Subsequently, the light beam traverses an analyzer positioned at -45° along the propagation direction, resulting in a polarized beam whose peak to peak amplitude is directly proportional to the reflectance difference between the orthogonal optical axes, [110] and [$1\bar{1}0$]. The spectral analysis of light is done by a monochromator (Jobin-Ivon MicroHR) with a focal distance of 140 mm and which has a diffraction grid of 900 lines per mm. A schematic description of the RDS optical setting is shown in Fig.3.

After the light beam emerges from the monochromator, the photons are collected by a 32-channel photomultiplier (Hammamatsu H7260). Each channel is sensitive to a defined wavelenght or energy of the photon. Then, the photoelectric effect describes the emission of electrons being accelerated toward an arrangement of dynodes where electrons are multiplied and directed to their respective anodes. As mentioned before, two RD spectrometer arrangements were used during this research, though the optical setting remained almost the same, the PEM of 50 kHz was changed by one of 90 kHz, the data acquisition differed in the receipt-send process from the lock-in to the PC, in the first case (a schematic diagram is shown in Fig. 4), the ΔR analogic signal is received serially (data by data, wavelength by wavelength) by the single channel lock-in [9], whereas in the second case, the signal is received in parallel (at the same time) by the 32-multichannel lock-in (Signal Recovery 7210 DSP), which is helpful in terms of increasing the data acquisition rate. At the same time, the signal to noise ratio is significantly increased over the previous spectrometer [10]. Whereas with the 50 kHz PEM arrangement, the maximum rate of spectra per second is of 1 spectrum per 200 ms, with the second arrangement, the rate is of 1 spectrum per less than 100 ms.

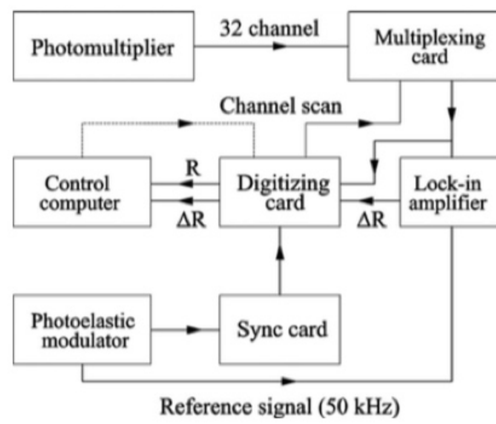

Figure 4: Electrical block diagram of the RD multichannel spectrometer. This figure is reprinted from reference [9].

2 THEORETICAL BACKGROUND

2.1 INTRODUCTION

In this chapter the different growth modes during epitaxial growth are defined in order to understand the deposition of InAs over GaAs(001). Also, this chapter introduces to the distinctive features that made possible the analysis of RDS and RHEED experimental results obtained along this work and which will be discussed in CHAPTER 3. Some of the aspects discussed in CHAPTER 2 are GaAs(001) surface reconstruction changes which come under two variables, the change in As overpressure, as well as the change of the substrate's temperature. This analysis is made in order to understand the changes that the GaAs(001) surface sustain during the deposition of InAs, as well as the evolution that the InAs surface covering suffers due to its continuous deposition. Also, the structural process that GaAs(001) surface undergoes during the deposition of InAs quantum dots (QD's) is seen from a STM perspective based on measurements taken by reference [5] for it to complementary the RD analyses done in this work and described in CHAPTER 3. Another of the aspects discussed in this chapter is the mathematical description of Singular Value Decomposition (SVD) and the importance of its application during the analysis of the spectra measured with the real-time RDS tool.

2.2 SEMICONDUCTORS GROWTH MODE

The mechanisms that lead to the different growth modes defined, are rather complex. They depend on the nature of the substrate (for example, crystalline vs amorphous), substrate temperature, deposition rate, flux energetics, impurities, and deposition geometry. In this section, an overview of some of the most commonly known mechanisms that lead to these different growth modes, is given. Understanding many of these formations is far from complete, so it is likely that the research in this area continues to be so for so many years to come.

The term epitaxy refers to a growth phenomena during which an accordance exists between the crystaline structure of the deposited film and the substrate where it is being grown. In a general way, it denotes the growth of a crystaline layer over a crystal surface. When the film and substrate materials are the same, the process is called homoepitaxy. If they are dissimilar, it is called heteroepitaxy. In the latter, it is common that the substrate and the growing film may have different lattice constants, which may cause a lattice mismatch during the growth, allowing it to change from one mode to another.

Epitaxial growth occurs only under sufficiently high substrate temperature and surface mobility (near equilibrium conditions). The morphology of the epitaxial film depends on a number of physical parameters, including the interfacial energy and lattice mismatch between

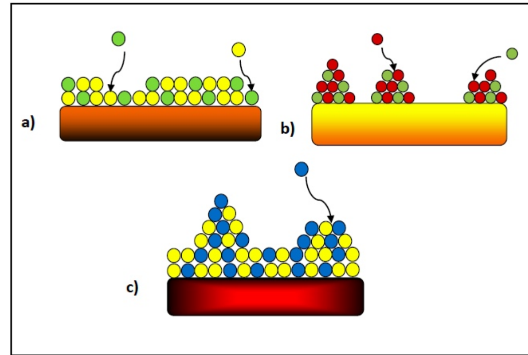

Figure 5: Schematic illustration of the three common epitaxial growth modes of materials, a) Frank-van der Merwe (FM), b) Volmer-Weber (VW), and c) Stranski-Krastanov (SK), growth mode.

the film and the substrate. There are three commonly known growth modes characterizing epitaxial growth morphology: Frank-van der Merwe (FM), Volmer-Weber (VW), and Stranski-Krastanov (SK) [15]. Figure 5 is a schematic illustration of these three growth modes.

During the FM or layer-by-layer growth mode, a single layer is nucleated on the substrate through the creation of two-dimensional (2D) islands [4]. In this growth mode the force between the film's adatoms and the substrate's is stronger than the internal forces between the film's adatoms. The growth continues to enlarge the islands until the whole surface is covered with the deposited material. A second layer is not allowed to nucleate until the completion of the entire first layer. In the VW growth mode, a large number of three-dimensional islands are grown before their lateral spreading. In this case the strength between the film's adatoms is larger than that between the substrate and the film, which originates the formation of these 3D islands. The SK growth consists of an intermediate case between FM and VW growth modes and is one of the most common. It is also known as "layer-plus-island growth". This growth modes name is due to the fact that initially the growth consists on a layer by layer growth until some critical thickness is reached giving way to an island growth mode or VW. Such critical thickness has a dependance on the lattice mismatch between the substrate and the film.The SK growth mode occurs when the lattice mismatch between the film and the substrate is large. The transition from FM to VW morphology is a result of island formation to reduce the strained energy caused by the lattice mismatch between a film and a substrate [4].

In the FM growth mode, the surface is atomically flat with some single atomic steps. A reflection high-energy electron diffraction pattern contains streaks that come from the diffraction of the electrons from the relatively flat surface [16]. For VW and SK growth, the films can be characterized by the RHEED transmission mode. The diffraction patterns reveal the structural properties of the films in the form of islands [4].

2.3 GAAS(001) SURFACE RECONSTRUCTIONS

Surface reconstruction refers to the process by which atoms at the surface of a crystal assume a different structure than that of the bulk. Surface reconstructions are important in the way that they help understanding the surface's chemistry for various materials, especially in the case where another material is adsorbed onto the surface.

In an ideal infinite crystal, the equilibrium position of each individual atom is determined by the forces exerted by all the other atoms in the crystal, resulting in a periodic structure. If a surface is introduced to the system by terminating the crystal along a given plane, then these forces are altered, changing the equilibrium positions of the remaining atoms. This is most noticeable for the atoms at or near the surface plane, as they now only experience interatomic forces from one direction. This imbalance results in the atoms near the surface assuming positions with different spacing and/or symmetry from the bulk atoms, creating a different surface structure. This change in equilibrium positions near the surface can be categorized as either a relaxation or a reconstruction.

2.3.1 GaAs(001) c(4x4) and (2x4) Surface Reconstructions

A variety of reconstructions has been found on the (001) surface of GaAs, ranging from the most As-rich c(4x4) , through (2x4) and some Ga-rich c(8x2) phases [17]. The simple picture of such reconstructions rests on the assumption of thermodynamic equilibrium: the surface is reconstructed in such a way that the surface energy is minimized. The sequence of structures on the GaAs(001) surface as a function of decreasing As coverage has been described elsewhere [18],[19] from the standpoint of the equilibrium of energy.

Surface structures of GaAs(001) grown by the MBE tecnique, change by varying the As overpressure as well as the substrate's temperature. The c(4x4) structure is usually observed under most As-rich environments, and has been widely believed to have three As-As dimers per unit cell, see Fig. 6 as well as references [20],[21]. On the other hand, a new structure model consisting of three Ga-As dimers instead of As-As dimers, see Fig. 6b has been recently proposed [20]. Based on reference [21], it can be assured that the kinetic dependence of GaAs c(4x4) surface reconstruction, depends on the As flux impinging the substrate, finishing the surface with a Ga-As dimer in the c(4x4)α surface reconstruction and an As-As dimer for a c(4x4)β surface reconstruction, those structures are formed when the surfaces are prepared using As_4 and As_2 molecules, respectively.

Whether the As flux used during a GaAs growth is As_4 or its molecules are dissociated into As_2, if the substrate's temperature is mantained in the wide range of 490-510° C, then the c(4x4)α phase will exist in either case, reference [21] can be checked out to understand this phenomena.

The fact that the diverse phases of a c(4x4) GaAs structure depend on temperature as well as on the As species being used can be characterized by RD spectroscopy as well as RHEED which show different but complementary and distinctive features of the surface reconstruc-

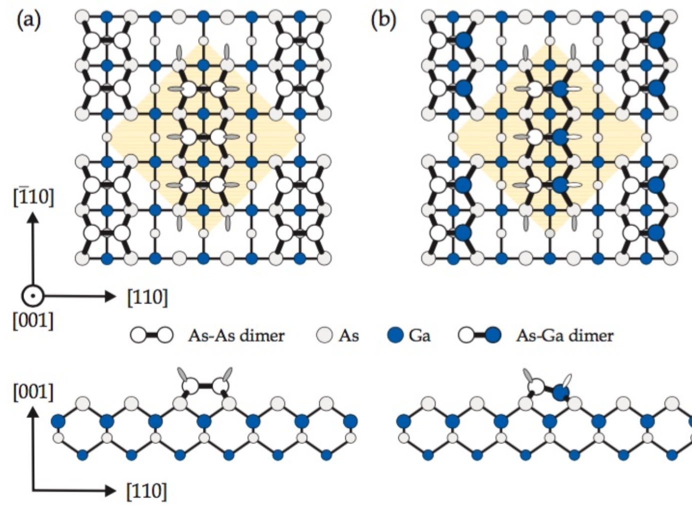

Figure 6: Top views and side views of the GaAs-c(4x4) reconstructed surface, in (a) As-As dimer configuration and (b) Ga-As heterodimer configuration. Filled As dangling bonds are depicted by gray ovals and empty Ga dangling bonds are depicted by white ovals. Atoms below the figure plane are depicted by smaller circles. For reasons of clarity the lower Ga atom plane is not shown in the top view images. This figure is reprinted from reference [5].

tions that GaAs is subjected to during homoepitaxial growth, as can be observed in Figures 7 and 8.

RDS technique is very sensitive to changes in surface crystallography, and has been demonstrated to be useful as a mean of characterizing the clean GaAs(001) surface under the environmental conditions encountered in molecular beam epitaxy growth processes. Distinctive features can be seen in the RDS spectrum of Fig.7, the characteristic spectrum of a GaAs c(4x4)α surface and its main transitions E_1 and $E_1 + \Delta_1$ are well defined at 2.61 eV and 2.81 eV respectively [22]. The evolution of these critical points with changes in temperature, can be seen as E_1 flips its sign from negative to positive when reaching the β_2(2x4) surface reconstruction and moving at the same time toward lower energies, around 2.57 eV for E_1 and 2.71 eV in the case of $E_1 + \Delta_1$. Nevertheless, RHEED diffraction patterns complement these information, as the surface reconstruction pattern changes indeed as it is seen in Fig.8, where the reciprocal lattice changes from half order in both directions [110] and [1$\bar{1}$0], to a 4x periodicity along the [1$\bar{1}$0] crystallographic direction and stays the same along [110], see Fig.9. These changes correspond to the characteristic lineshapes seen with RDS in Fig.7C and Fig.7A, respectively.

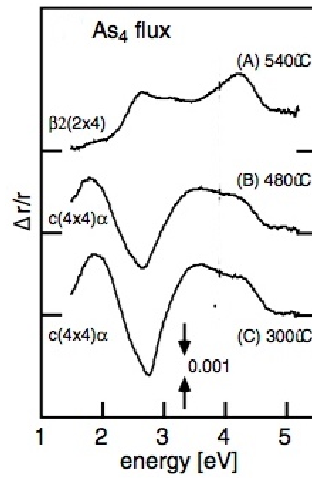

Figure 7: Evolution of RD spectra measured during the growth of GaAs/GaAs under an As_4 flux. Figure taken from reference [21].

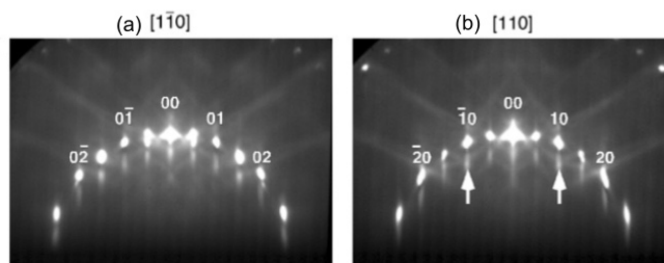

Figure 8: RHEED Diffraction Patterns of GaAs c(4x4) reconstruction. Figure reposted from [23].

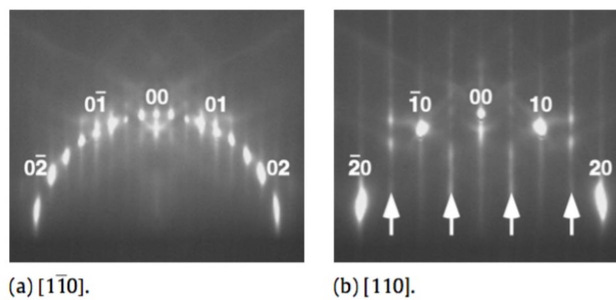

Figure 9: RHEED Diffraction Patterns of GaAs (2x4) reconstruction. Figure reposted from [23].

2.4 CHARACTERIZATION OF INAS/GAAS(001) GROWTH

InAs is a low-band-gap (E_g=0.36 eV, compared to 1.42 eV for GaAs) compound semiconductor material with a zinc blende structure (as well as GaAs) and promising for applications in high-speed transistors, infrared detectors, and lasers. The InAs/GaAs materials system is a particularly challenging candidate for the study of heteroepitaxial growth owing the large lattice mismatch (7.26%) betwen GaAs and InAs, being a growth with an ideal environment to the formation of quantum dots (QD), which are structures that self-form due to the transition of the growth mode from 2D to 3D at a certain layer thickness.

2.4.1 Studies of InAs Quantum Dot Growth

2.4.1.1 *InAs/GaAs(001) RD Spectra Characterization*

In the study made in reference [24], RDS optical spectra of InAs growth over GaAs(100) were measured during a stepwise deposition (of 0.5 ML per step). A significant change in sign in the RDS signal at about 2.6 eV (the As dimer-related energy on GaAs) is clearly observed even for sub-monolayer coverage, see Fig.10. An instantaneous reconstruction change from an As-rich c(4x4) GaAs surface to a (1x3) InAs reconstructed surface was reported from MBE growth, where simultaneous RHEED measurements were performed. With an increasing amount of InAs on the surface, the anisotropy increases and the structure in RDS shows a redshift displacement.

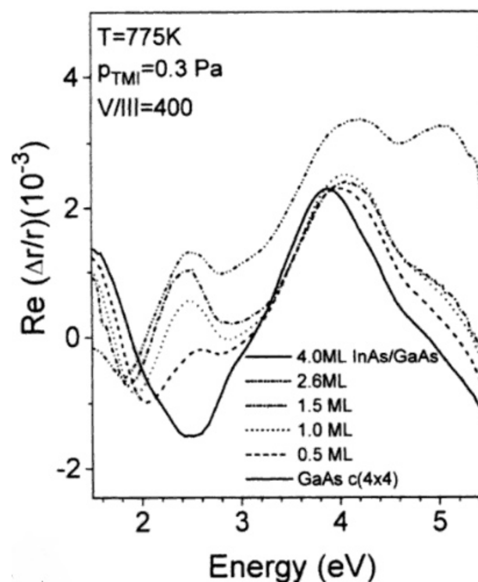

Figure 10: RDS anisotropy spectra measured after the stepped deposition of well defined amounts of InAs on GaAs(100). Figure reposted from [24].

Such study is complementary to the results obtained during the time-resolved observation of RDS signal during the deposition of InAs made in ref.[25] and centered around 2.5 eV. Here, the authors observed a bump during early stages of InAs deposition and related it to the decrease of surface anisotropies with the increasing of temperature (the bump is not seen at lower temperatures as can be seen in Fig.11). This feature is indicated by them by solid bars at which the c(4x4) RHEED pattern (study made during these experiments) completely disappears and the further deposition of InAs results in the formation of the (1x3) surface reconstruction. Besides, the RD signal at 2.5 eV shows the sign inversion and the intensity converges to a constant positive level for the (2x4)α2. It is noted that the positive signal starts to saturate during the growth transitions, which means that the disappearance of the excess As surface triggers the islanding process (see the black arrows in Fig.11).

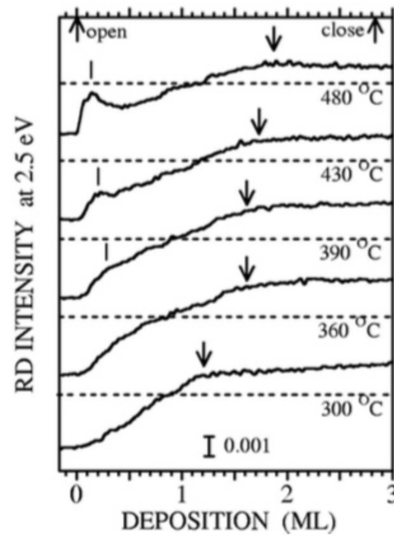

Figure 11: Time-resolved RD intensity at 2.5 eV. The arrows indicate the growth transitions. Figure reposted from [25].

2.4.1.2 *InAs QD's/GaAs STM Surface Reconstruction Characterization*

Additionally, reference [5] reports a structural analysis with Scanning Tunneling Microscopy (STM) which was measured during the deposition of increasing amounts of InAs. InAs thin films were grown on different GaAs(001) samples in a c(4x4) surface reconstruction. During the experiment, the As_2 overpressure was of 2.6x10^{-6} Torr and the substrate's temperature was 460° C. In figures 12 and 13, are shown a pair of STM images of samples that were grown during the experiment with different InAs coverage, 0.09 ML and 0.56 ML , respectively. During this study, they concluded that though the lack of sharpness of the STM images, the In atom configuration might be supported by a model where the surfaces dissolutes its initial c(4x4) surface to replace it with an InGaAs (nx3) reconstructed surface. This due to the increasing density of the InAs signatures which requires further surface space at the cost of the As top dimers in between, as a result, it exists no more a given symmetry pattern (c(4x4)) from the underlying initial surface. Instead the transformation to another surface configuration, as it is an InGaAs (nx3), might be energetically preferable during chemisorption. One of

the samples where 1.65 ML of InAs were grown, was analyzed observing that after the initial GaAs c(4x4) surface reconstruction was dissoluted, it was replaced by a wetting layer (WL) of $In_{2/3}Ga_{1/3}As$-(4x3) (see Fig.14) reconstruction which evolves to a further coverage by a second (2x4) reconstructed InAs layer as In continues to add to the surface. Such reconstruction arrangement, was derived from the STM images, where an average of different domains zones were observed. Structural models for these α2-(2x4), α2-(2x4)-m and β2-(2x4) reconstructions are presented at Fig.15. These models are all in very well agreement with the observed STM data. At a completed two layer WL, the critical thickness and the 2D→3D transition took place causing the formation of the QD's precursor states due to strain relief providing attractive sites for further InAs accumulation. During this process, the precursors evolve to QD's (ripening) by accumulating material from the WL as well as from the molecular beam. A significant density of QD's must evolve before they can visibly contribute to the RHEED diffraction patterns. The fast quenching of the sample immediately after material deposition interrupts this process and both QD's as well as precursors are observed, even though there might not be clear evidence for QD's in the diffraction patterns.

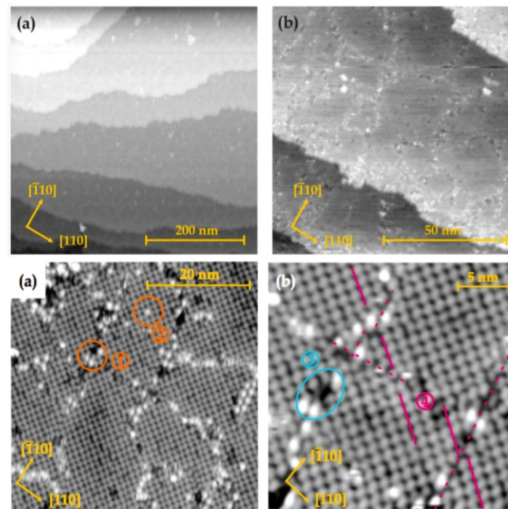

Figure 12: STM images of the GaAs(001) c(4x4) reconstructed surface covered with .09 ML of InAs. Upper image: (a) exhibits a smooth surface with flat terraces, the more detailed view in (b) reveals large areas of GaAs c(4x4) reconstruction and a mesh with signatures of bright contrast caused by the deposited InAs. Lower image: The image in (c) illustrates the preferential adsorption sites for the InAs, marked by orange circles. (d) the InAs surface structure defects and dislocations are evident, coexisting domains of a nearly undisturbed GaAs c(4x4) surface. Figure reposted from reference [5]

Strain effects during the evolution of the InAs wetting layer

The effects of strain during the growth of the InAs wetting layer was also discussed and modeled during the study described above. The structural models proposed were based on the strains due to the bond lenghts of the surface atoms.

First, authors assume that there is a tensile strain due to the triple dimer As-As blocks in the surface. Such strain is caused because the bonds of such dimmers are 1.5 times smaller than

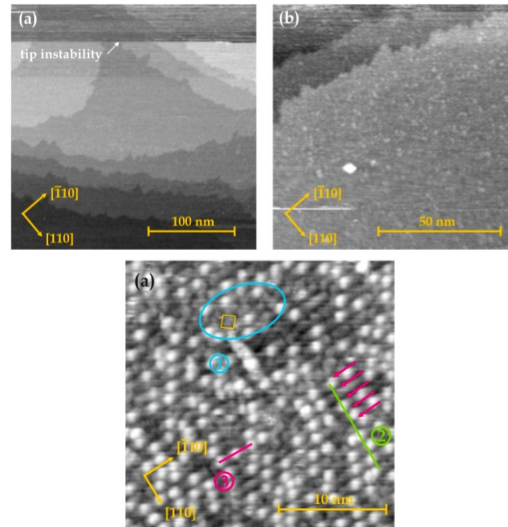

Figure 13: STM images of GaAs(001) c(4x4) reconstructed surface covered with 0.56 ML of InAs. Upper image: (a) shows a smooth surface with large terraces. In the more detailed view in (b) the initial c(4x4) is not clearly evident any more, and the observed InAs signatures are now distributed evenly over the surface. Lower image: More resolved image showing a uniform distribution of the InAs signatures. Figure reposted from reference [5].

the bulk As bonds. This direction of the strain goes along the dimer bond direction, i.e. [110]. Besides there's also a second tensile strain along the [$\bar{1}$10] direction, due to the difference in atomic bond lenghts between the As dimers top layer and the As atoms underneath, which is shorter than the bond lenghts between the Ga-As bond lenghts in the bulk. There is a trench formed (see Fig.16) between the As triple dimer rows and the next unitary cell (depicted in yellow at the figure), which prevents the surface from accumulating significant surface strain.

When the In atoms start to incorporate to the GaAs surface in the center of the hollow site, marked by ①, it causes a moderate compressive strain along the [$\bar{1}$10] due to the larger In-As bond lenght (.262 nm) as compared to the Ga-As bond lenght (.243 nm). Such strain, partly compensates the tensile strain at the As triple dimer blocks. That tensile strain is even reduced more by the incorporation of four further In atoms placed within the outer dimer As-As backbonds, marked by ② in Fig.16. The same incorporation of those In atoms within the trenches also contributes to reducing the strain accumulation along the [1 1 0] direction as well.

There is also strain in the $In_{2/3}Ga_{1/3}As$ (4x3) reconstructed monolayer stage. If seen along the [1 1 0] direction, three atomic rows build up the InGaAs (4x3) surface, above the bulk GaAs bonds, two rows of In alternate with one row of Ga, causing a compressive strain towards the Ga atom in between, this due to the smaller atomic bond of In-As compared to the Ga-As one (see the right side view of Fig.17) . Still analyzing the same crystallographic direction, the As dimers along the trench formed between unitary cells, are relaxed outward the surface. This relaxation of the In atoms allows the As dimers of the third layer to form above the Ga rows as this shift allows the dimer bonds to relax towards their natural bond lenghts. Then the compressive strain of the $In_{2/3}Ga_{1/3}As$ atoms along the [110] direction, allows the neighboring In

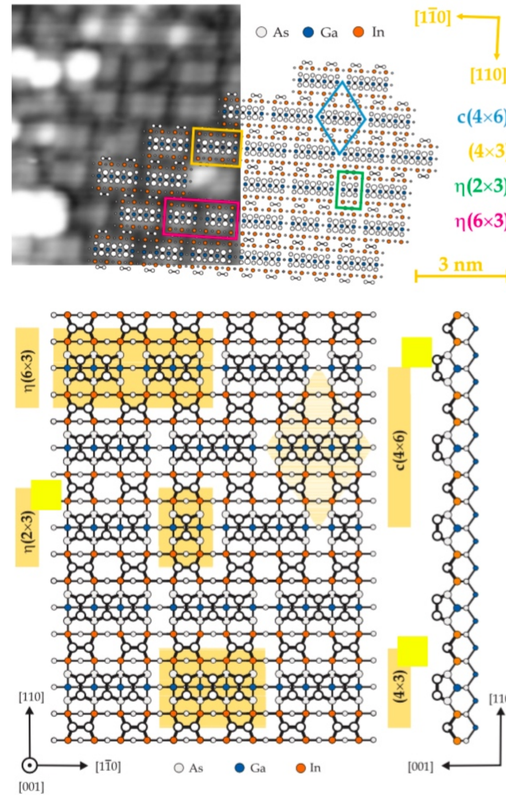

Figure 14: Top: STM image of the (4x3) reconstructed $In_{2/3}Ga_{1/3}As$ ML overlaid. Bottom: Top view and side views of the proposed structural model of the (4x3) reconstructed $In_{2/3}Ga_{1/3}As$ ML. Atoms below the figure plane are depicted by smaller circles. The different observed surface unit cells are marked by yellow boxes. Figure reposted from reference [5]

atoms to partly relax towards the Ga bulk positions. The shorter distance between adjacent As atoms on top of the Ga atoms is favorable for the formation of As-As top dimers, as it fits well to their shorter bond length.

Analyzing the [$\bar{1}$10] direction, compressive strain of the In atoms rows over the GaAs bulk lattice is accumulated, due to their bigger atomic radius. At the same time, the shorter As-As bonds of the 3 dimer blocks, cause tensile strain over the GaAs bulk lattice, causing the As dimers to shift together and form the hollow sites at every fourth dimer position to relax such strain. Both processes are illustrated by green arrows in the lower side view of Fig.17. It is highlighted that during this stage the hollow sites provide the only possibility for a strain reduction of the As triple dimers, causing such periodicity to be considerably large and stable.

When the InAs (2x4) reconstructed layer starts to develop, the As dimers of the underlying (4x3) reconstructed $In_{2/3}Ga_{1/3}As$ will not contribute to the strain anymore. There are three InAs (2x4) reconstructions, as seen in Fig.18, the [$\bar{1}$10] alternating $\alpha 2(2x4)$ and $\alpha 2(2x4) - m$ reconstructions, as well as the less seen $\beta 2(2x4)$, which contribute to the total strain in the sur-

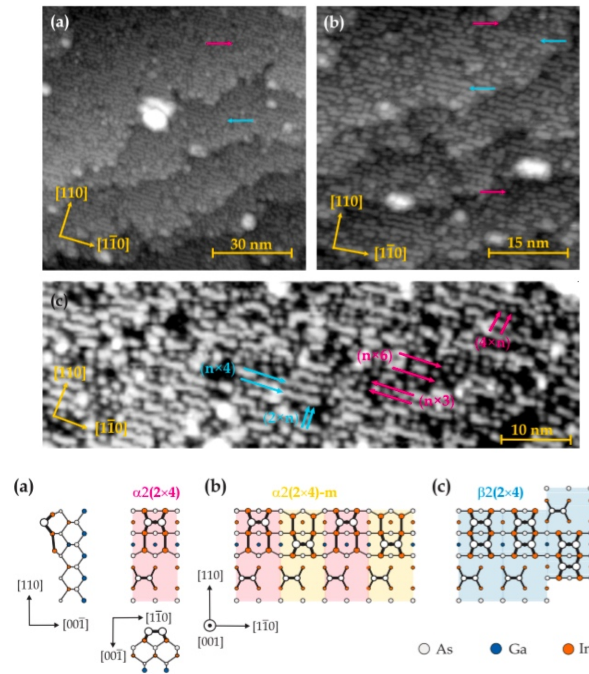

Figure 15: Above: STM images of the InAs WL, which apparently consists of two layers, on which two different reconstruction patterns are observed. The upper layer (blue arrows) is congruent to the InAs(2x4) reconstruction, althought this layer does not cover the entire surface. The locally uncovered layer underneath (magenta arrows) is congruent to the InGaAs(4x3) reconstruction. In (c) the corresponding surface periodicities are shown with more detail. Below: (a) Top view and side views of the InAs $\alpha(2x4)$ surface unit cell. (b) Zig-zag alignment of the $\alpha 2/\alpha 2$-m configuration. (c) In-line alignment of $\beta 2(2x4)$ surface unit cells and an occasionally observed mirror alignment corresponding to the threefold symmetry of the trench dimer of the underlying $In_{2/3}Ga_{1/3}As$ ML. Atoms below the figure plane are depicted by smaller circles. Figure reposted from reference [5].

face. In the [110] direction the tensile strain is caused by the shortness of the As-In backbond lenghts, and also the formation of In-In bonds which are characterized by a length factor of .70 compared to the distance of two As atoms of the GaAs bulk. Both effects allow compensation of the mentioned compressive strain contributions from the underneath $In_{2/3}Ga_{1/3}As$ layer.

Along the [$\bar{1}$10] direction the zig-zag signatures of the alternating $\alpha 2(2x4)$ and $\alpha 2(2x4) - m$ reconstructions, exhibit a much larger compressive strain than the c(4x4) and the (4x3) reconstructed structures previously discussed.

All those surface configurations mentioned before, compensate the accumulated strain energy. Yet, during the InAs (2x4) coverage a significant amount of compressive strain remains along the [$\bar{1}$10] direction still remains. At this point the wetting layer contains 1.42 ML of InAs, any further InAs deposition will rapidly induce more compressive strain, in such situation the transition from 2D to 3D growth allows the relaxation of the compressive strain. And it is when the occurrence of the QD formation starts. Additionally, further deposited InAs as well

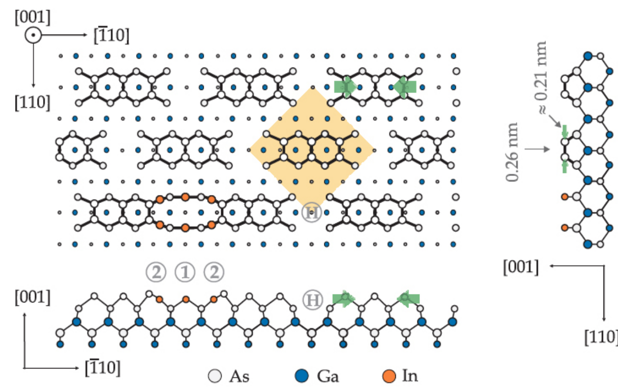

Figure 16: The model illustrates the structure of the initial empty hollow sites and a hollow site occupied by one of the InAs signatures.The strain effects are illustrated by green arrows. The surface unit cell is marked by a yellow box. Figure reposted from [5].

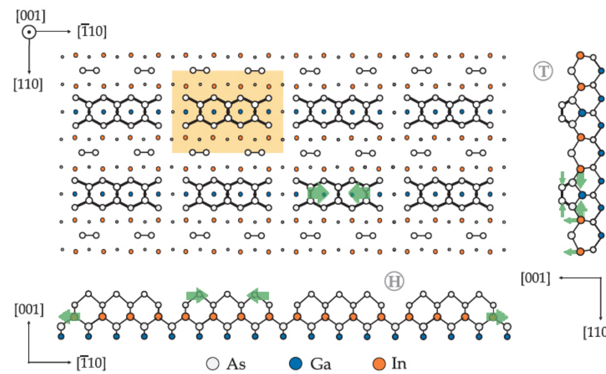

Figure 17: The strain induced hollow site between the As dimer blocks is marked by Ⓗ, the characteristic As trench dimer site is marked by Ⓣ.The respective strain effects are illustrated by green arrows. Figure reposted from [5].

as material from the WL start relocating into the QD's.

2.4.1.3 *InAs QD's /GaAs(001) AFM and RHEED Height and Density Characterizations*

There are other important features to study during the evolution of InAs QD's in real-time, the changes in the amount of them per area (density) and the changes in shape or size. These features are characterized by the use of techniques such as AFM and RHEED. During the follwing study, RHEED was used to characterize the changes (such as density and size) that the surface suffered during InAs quantum dots deposition. The study was divided in two phases, during the first phase a positive very slanted slope is obtained from RHEED's intensity lineshape, such change corresponds to a QD's density augmentation and it comprises the range from 1.5 ML to 1.8 ML along the [110] crystallographic direction (see purple slope in Figure 19a, taken from reference [26]). It is also seen in the range from1.6 ML to 1.9 ML along the opposite

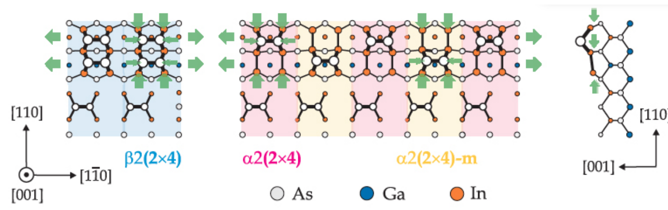

Figure 18: At the β2(2x4) configuration, the comparatively short As-In backbond length of the As dimers causes a moderate tensile strain, compensating the compressive strain in the [110] direction originating from the $In_{2/3}Ga_{1/3}As$ layer underneath. The formation of In-In dimer bonds at the $\alpha 2/\alpha 1 - m$ configuration intensifies the tensile strain in the [110] direction and thus the compensation of the compressive strain resulting from the underneath layer. In the [$\bar{1}$10] direction, the tensile strain from the As top dimers cannot sufficiently compensate the compressive strain caused by the comparatively larger In atoms. Thus with the increasing the (2x4) coverage, a significant amount of strain energy is accumulated, finally resulting in QD growth. The respective strain effects are illustrated by green arrows. Figure reposted from reference [5].

crystallographic direction, [1$\bar{1}$0]. The second phase of the growth is defined by another change in slope (see cyan slope in the same figure) which describes the increasing height of InAs QD's instead of their density as was stated before. These conclusions were supported by an AFM characterization, which can be seen in Figure 19b where a visual idea of the change in density with total deposition is given; (a) 1.6, (b) 1.8, (c) 2.0, and (d) 2.5 ML are 250, 580, 880, and 900 μm^{-2}, respectively. From a quantitave analysis, the average height distribution of the QDs for different deposited amounts of InAs, is in (a) 1.6, (b) 1.8, (c) 2.0, and (d) 2.5 ML, corresponding to the heights of 2.0, 2.1, 2.5, and 2.8 nm, respectively. The average heights are almost identical for 1.6 and 1.8 ML. However, the heights increase when the InAs deposition reaches an amount of 1.8 ML. These AFM images suggest that the density of QD's have a direct relation with the amount of InAs deposited during the first slope whereas the density does not change during the second slope and instead the size of the QD's do.

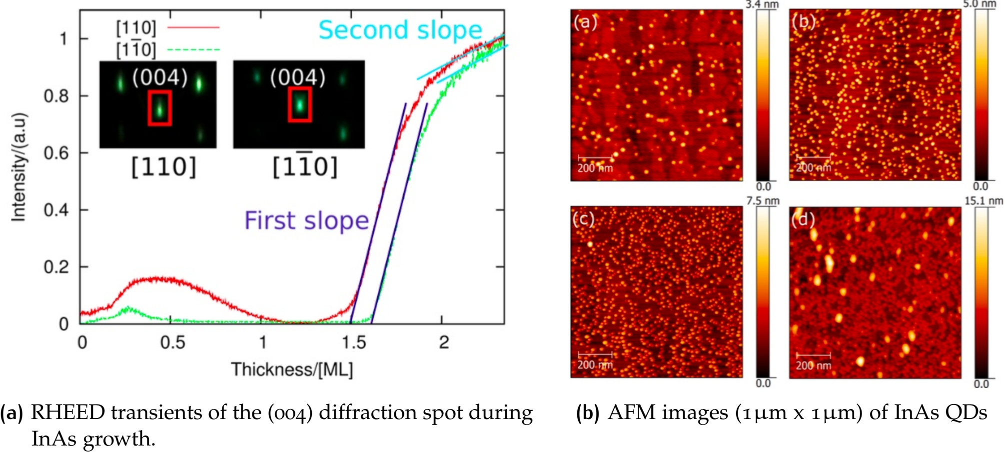

(a) RHEED transients of the (004) diffraction spot during InAs growth.

(b) AFM images (1 µm x 1 µm) of InAs QDs

Figure 19: Left: RHEED transients at the (004) diffraction spot along the [110] and [1$\bar{1}$0] incident azimuth during InAs growth. The corresponding RHEED patterns observed after 2.5 ML InAs deposition are shown in the inset. Right: AFM images (1µm x 1µm) of InAs QDs grown after different amount of deposition: (a) 1.6 ML, (b) 1.8 ML, (c) 2.0 ML, and (d) 2.5 ML. The substrate temperature during growth is 480°C. Figure reposted from reference [26].

2.5 SINGULAR VALUE DECOMPOSITION AND RDS SPECTRA

One of the most useful results from linear algebra is a matrix decomposition known as the singular value decomposition. In this section, the theory behind this matrix decomposition will be explained to understand how this powerful mathematical tool can be applied to the RD spectra analysis finding an interpretation to the physical phenomena taking place during the heteroepitaxial growth.

2.5.1 SVD applied to Real-Time RDS spectra

As it is described in Appendix A, the mathematical tool of Singular Value Decomposition (SVD) is powerful due to its capability of finding a set of vectors that form an orthonormal basis which, with the appropiate combination, will comprise each of the vectors of the experimentally measured in this work. Such orthonormal basis can be compared to the 3-Dimensional coordinate system composed by 3 orthogonal axes, x, y and z. Using a linear combination of the three orthogonal axes, a three-dimensional vector is created as seen in Fig.20. In this example, such three-dimensional vector stands in the place of one of the RD measured spectra, and it is comprised by a linear combination of the 3 orthogonal axes (x, y, z), which in the case of the spectra, each axis corresponds to a lineshape obtained by SVD (see Figure 21a), and by combinating each other among them, they will form the experimental spectra (see Figure 21b).

Returning to our 3-Dimensional system, its difference between the RD measured spectra, is that meanwhile the 3D coordinate system comprises of three orthogonal bases, which combined form the vector $\vec{v} = x\hat{\imath}+y\hat{\jmath}+z\hat{k}$, represented in Fig.20, each of the RD spectrum is com-

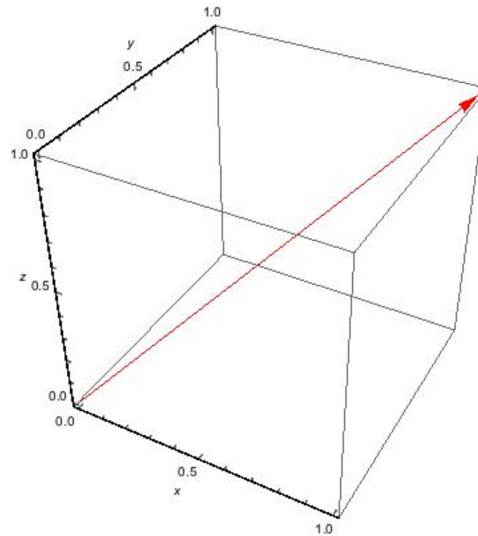

Figure 20: The 3-Dimensional cartesian system and a vector formed by a linear combination of each of the bases that comprise the system.

prised by one measured value per wavelength, being in this case, 32 measurements along 32 different wavelenghts, the spectra (measured data is shown as example in Figure 22a) then can be arranged in matrix A of 32xn. If this matrix submits to a SVD analysis, it is possible to obtain its singular values (as it is seen in 22b), which will be the orthogonal bases needed to fit each of the experimental spectrum.

Lets consider the following matrix **A** as our arranged measured experimental spectra, decomposing it into its singular values, it can be rewritten as the product **A= U**ΣV^T of the three matrices, **U**, Σ, and $\mathbf{V}^T$, where U and V have orthonormal columns and Σ **is a diagonal matrix whose entries are known to be the singular values of A.** Such eigenvalues are ordered from the biggest amplitude ones to the less important ones (as are represented in Figure 22b, being the colored spectra the most important ones and the black ones the less important). Each of the matrices correspond to the following, the diagonal matrix Σ, which has σ_i eigenvalues on the diagonal; the matrix U with r_i's as columns; and the matrix V with x_i's as the columns;

$$U = \begin{bmatrix} r_{1i} & r_{1i} & r_{1i} & \dots & r_{1n} \\ r_{2i} & r_{2i} & r_{2i} & \dots & \dots \\ r_{3i} & r_{3i} & r_{3i} & \dots & \dots \\ \dots & \dots & \dots & \dots & \dots \\ \dots & \dots & \dots & \dots & \dots \\ r_{32i} & r_{32i} & r_{32i} & \dots & r_{32n} \end{bmatrix} \Sigma = \begin{bmatrix} \sigma_{i1} & 0 & 0 & \dots & 0 \\ 0 & \sigma_{i2} & 0 & \dots & 0 \\ \dots & \dots & \sigma_{i3} & \dots & 0 \\ 0 & 0 & 0 & \dots & \sigma_{i32} \end{bmatrix}$$

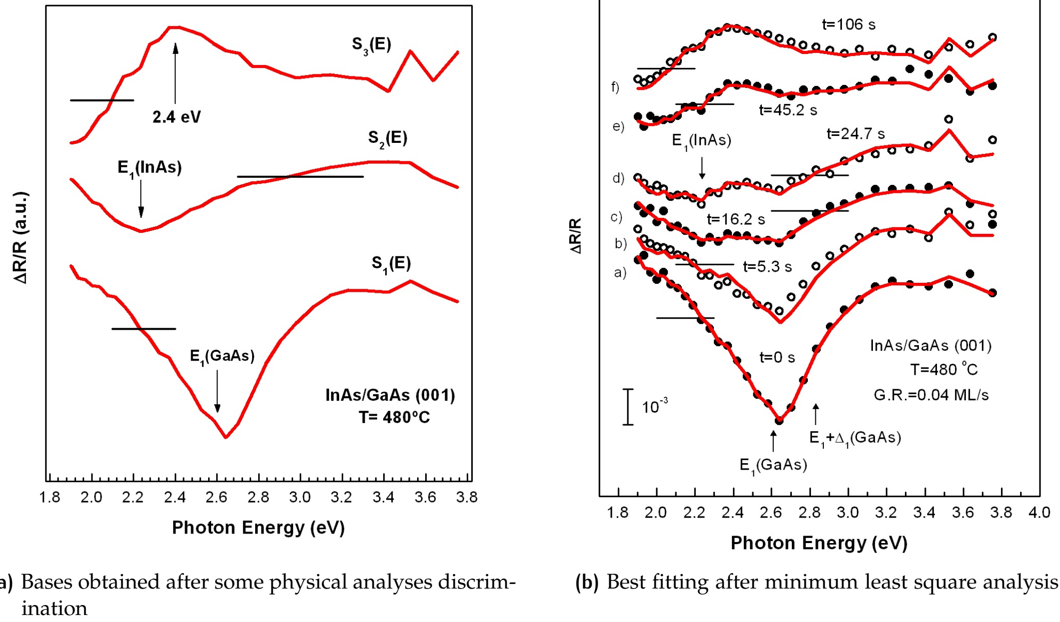

(a) Bases obtained after some physical analyses discrimination

(b) Best fitting after minimum least square analysis

Figure 21: Left: Bases obained after discriminating 2 of the five shown in previous figure due to its non-physical meaning. Right: The best fits of the combination of such bases to the experimental spectra, due to a minimum least square analysis.

$$V = \begin{bmatrix} x_{1i} & x_{1i} & x_{1i} & \dots & x_{1n} \\ x_{2i} & x_{2i} & x_{2i} & \dots & \dots \\ x_{3i} & x_{3i} & x_{3i} & \dots & \dots \\ \dots & \dots & \dots & \dots & \dots \\ \dots & \dots & \dots & \dots & \dots \\ x_{32i} & x_{32i} & x_{32i} & \dots & x_{32n} \end{bmatrix}$$

Where x_i are the right eigenvectors of A , with λ_i as the eigenvalues. And where $\sigma_i = \sqrt{\lambda_i}$ and $r_i = A\ x_i / \sigma_i$.

The corresponding eigenvectors and eigenvalues of A, are obtained by calculating the eigenvalues of either matrix U or matrix V^T, as it is explained in Appendix A. Although 32 orthonormal eigenvectors with 32 corresponding eigenvalues, result from the SVD analysis, not each of those 32 eigenvectors are used as part of our mathematical bases. Such discrimination is done due to the amplitude of each calculated vector. Some of them are so small that are not needed to be taken into account in the path of finding those bases that will actually have a real physical meaning during the heteroepitaxial growth. Fig.22b represents this situation in a graphic way.

In Fig.22b a graph of the 32 orthogonal eigenvectors is shown. Each of the vectors (spectrum) is graphed in their real scale, making it obvious that due to such amplitude only three of those

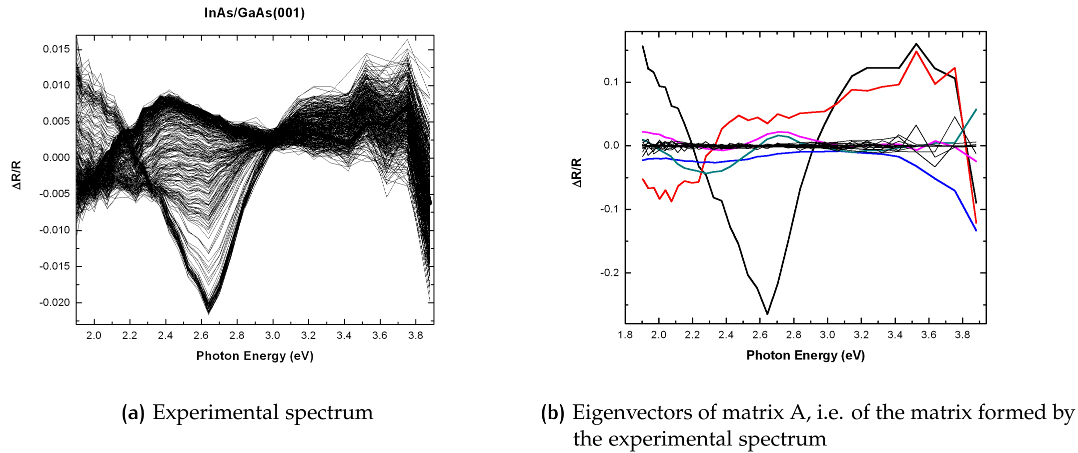

(a) Experimental spectrum

(b) Eigenvectors of matrix A, i.e. of the matrix formed by the experimental spectrum

Figure 22: Experimental RD spectra which are to be arrenged in a matrix **A** of 32xn to obtain its singular values by an SVD analysis. a) Experimental RD spectra, b) Singular values

32 vectors have equiparable weights and are taken into account to comprise each of the RD measured spectrum by means of linear combinations (as it was stated before), which will be explained next and which is being observed in Fig.21b.

On the basis of the above discussion, the time-dependent RD spectrum is written as S(E,t), so the corresponding eigenvalues calculated before by SVD compose each of the S(E,t) spectrum by a linear combination of them as it is described in equation 2.1:

$$S(E,t) = c_1(t)S_1(E)+c_2(t)S_2(E)+c_3(t)S_3(E) \tag{2.1}$$

Where $c_i(t)$ are the corresponding coefficents of each base, or spectral component. The interesting stuff comes in determining coefficients $c_i(t)$ and thus the time-evolution of components $S_i(E)$. Once the basic spectral components were determined, $c_i(t)$ coefficients were calculated through a minimum least square fit of Eq. 2.1 to the whole series of time-dependent experimental spectra [27].

However, even though SVD spectra analysis is a completely useful mathematical technique, it just serves as a guide to obtain the spectral components, as a mathematical agreement, not necessarily means a physical meaning. As it is observed in Fig.22b and Fig.21a, where the five bases given by the SVD analysis were reduced to only three due to its lack of physical meaning. So, further intuitive studies which mainly base on preconceived and strongly proved ideas, lead to the model of such spectral components (or a variation of them), using the strain model or a roughness model in some cases. Done this, the semiconductor growth may has a sustentation on real physical phenomena.

In summary;

- Singular Value Decomposition (SVD) is a factorization of a real or complex matrix

- A M matrix with an order of 32xn is comprised by each experimental measured spectrum.
- M is composed by 3 matrixes; $U\Sigma V^*$
- U is a 32x32 matrix whose columns are called left singular vectors.
- Left singular vectors are a set of orthonormal eigenvectors of MM^*
- Σ is a 32xn matrix whose diagonal entries σ_i are known as the singular values of M.
- V is a nxn matrix whose columns are called right singular vectors.
- Right singular vectors are a set of orthonormal eigenvectors of M^*M
- The non-zero singular values of M (found on the diagonal entries of Σ) are the square roots of the non-zero eigenvalues of both M^*M and MM^*
- The Σ matrix is composed by the eigenvectors obtained which are ordered in descending order of amplitude.
- Each of the eigenvectors in the matrix Σ corresponds to a spectrum in Fig. 22b where the ones with the biggest amplitude are highlighted in color.

2.6 RECONSTRUCTION-INDUCED STRAIN AND RDS SPECTRA

Under applied forces, solids are strained resulting in a change of volume and shape. Whereas these are external forces or forces due to surface reconstructions, both of them can be characterized using the Reflectance Difference Spectroscopy measurement technique, as it is shown in the following references [28],[29] for GaAs:Cr (100) by in-plane dislocations or surface electric fields in the first case and GaAs(001) homoepitaxy growth for the second case.

RDS measurements of the (001) surface of GaAs crystals have shown that the relaxation of the position of surface atoms induces an anisotropic strain which penetrates several atomic layers into the bulk, leading to optical surface anisotropy [30],[31],[32].

In the energy region around the E_1 and $E_1 + \Delta_1$ transitions, the RD spectra of c(4x4) and (2x4) GaAs surfaces are predominantly determined by the reconstruction-induced component of the strain. Such strain has the same orthorhombic symmetry as that resulting from the application of an external uniaxial stress along the [110] crystallographic direction, but with some differences in RDS line shapes [29].

From previous published articles, it is known that the line shape of the GaAs bulk's dielectric function at room temperature is dominated by discrete excitonic transitions [33],[34]. However, in reconstructed surfaces, there is a piezoelectric field, induced by the surface strain, which could ionize the excitons quenching its contribution to the RD spectrum and rendering the 2D contribution to be relatively more important [29].

Based on reference [29], the stress tensor and its relation to Reflectance Difference Spectroscopy and the Dielectric Function, will be described to correctly justify the fitting of RD measured spectra to this model, which will be described in the Experimental Results Chapter.

2.6.1 Linear Model

Assuming normal incidence, equation 2.2 corresponds to the lineshape for RDS that describes a surface strain-induced due to reconstructed surfaces of GaAs (001)] around E_1 and $E_1 + \Delta_1$ transitions, and it can be understood by assuming a surface strain and a change in the character of the transitions from discrete-exciton to one-electron (band to band two dimensions) [35].

$$\frac{\Delta R}{R} = Re[(\alpha - i\beta)\Delta\tilde{\phi}] \tag{2.2}$$

Where α and β are the Seraphin coefficients and $\Delta\tilde{\phi}$ is the contribution of the complex dielectric function. In the following equation the complex dielectric function is in terms of its polarization along [110] and [$1\bar{1}0$] crystallographic axes, $\Delta\tilde{\varepsilon}'$ and $\Delta\tilde{\varepsilon}''$, respectively; ϕ' and ϕ'', correspond to the phases which account for the fact that light penetration depth is larger than the thickness of the subsurface anisotropic layer [29],[36],[37].

$$\Delta\tilde{\phi} = e^{i\phi'}\Delta\tilde{\varepsilon}' + e^{i\phi''}\Delta\tilde{\varepsilon}'' \tag{2.3}$$

The difference in overall dielectric function is given by [38]

$$\Delta\tilde{\varepsilon} = \frac{D_1^5 S_{44}}{4\sqrt{3}}\frac{1}{E^2}\frac{\partial(E^2\tilde{\varepsilon})}{\partial E}\gamma + \frac{2D_5 S_{44}}{\sqrt{6}\Delta_1}(\tilde{\varepsilon}' - \tilde{\varepsilon}'')\gamma \tag{2.4}$$

where S_{44} is the elastic compliance modulus, D_1^5 is the interband orthorhombic deformation potential, D_5 is the valence band orthorhombic deformation potential, Δ_1 is the valence band spin-orbit splitting, and γ= aLX, where a is the optical absorption coefficient, L is the thickness of the strained region, X is the average uniaxial surface stress and $\tilde{\varepsilon}'$ corresponds to the E_1 and $\tilde{\varepsilon}''$ to the E_1+Δ_1 critical points [36].

As it was stated before, due to the fact that the thickness L of the anisotropic region induced by the surface strain is lower than the penetration depth of the probing light around the E_1 transitions, the surface dielectric function for fully ionized excitons, is described by the 2D line shape given by

$$\epsilon' = Ae^{i\theta}\ln(E - E_g + i\Gamma) \tag{2.5}$$

$$\epsilon' = Ae^{i\theta}(E - E_g + i\Gamma)^{-1} \tag{2.6}$$

In equations 2.5 and 2.6, E_g corresponds to the bandgap energy and Γ corresponds to the broadening parameter. The phase angle θ in equation 2.5 describes the metamorphism of 2D critical-point line shapes due to excitonic effects [33]; an angle θ = 0 corresponds to one-electron transitions. The excitonic metamorphism increases the value of θ [33] being such effect described by equation (2.6).In other words, the phase angle is interpreted as a coupling parameter between the discrete exciton interaction with an overlapping continuum of inter-band transitions [33]. There is also a temperature dependence between the optical constants

and the critical-point parameters of undoped GaAs for temperatures from 20 to 750 K in the photon-energy range from 1.3 to 5.6 eV, which was measured by P. Lautenschlager [33], in 1987, and which was taken into account for the corresponding fits in Chapter 3. In such publication, depicted in the next figure, Fig.23, it was observed a decrease of the excitonic phase angle passing from positive to negative, indicating that excitonic interaction decreases with increasing temperature, but does it necessarily disappears?

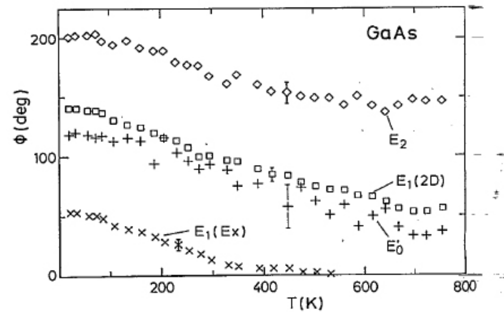

Figure 23: Temperature dependance of the phase angle θ defined in Eqs.(2.5) y (2.6) for E_1 transitions, fitted with an excitonic, x, and a 2D line shape (square).

In Fig.24, taken from reference [29], are shown the RD spectrum evolution as reconstruction changes gradually from c(4x4) to (2x4) as GaAs is deposited in a surface of GaAs(001), the contribution of the surface strain to the line shape was identified and fitted with a 2D inhomogeneous-strain model, as expected.In Fig.24a, it is as well, shown a spectra due to unixial stress with its corresponding excitonic lineshape.

It is observed in that same figure that from the c(4x4) reconstruction, spectrum (a), its amplitude decreases monotonically (see Fig.24a, spectra (a) to (c)), becoming almost quenched as it is seen in spectra (d) and (e). Showing the condition of zero strain lies between the curves (d) and (e) [39],[40],[41]. Beyond this point, the amplitude increases monotonically with an opposite sign to that of the initial spectrum (see spectra (e) to (f)). In those spectra, around 2.55 and 2.8 eV, a weak, changing slope structure took place with the evolution of the spectra. Such structure is due to transitions between occupied bulk valence-band states and empty surface states [42],[43],[44].

Fig.24b shows the RD spectrum of Fig.24a (hollow circles) along with the corresponding fit (solid line) performed on the basis of an inhomogeneous perturbation (small thickness L of the anisotropic region induced by the surface strain compared to the light penetration depth). In such case, they use a phase angle of $\theta = 70^{o}$ to fit the dielectric function. An independent angle of $\theta = 0^{o}$ was used for the RDS lineshape. These zero values are indicative of exciton quenching near the surface due to the surface electric field. It is important to note that although bulk exciton effects increase when lowering the temperature, as indicated by the increase in θ required for the dielectric function to fit, the phase angle θ used to fit the RD line shape is relatively independent of temperature. This result is expected if it is considered that the

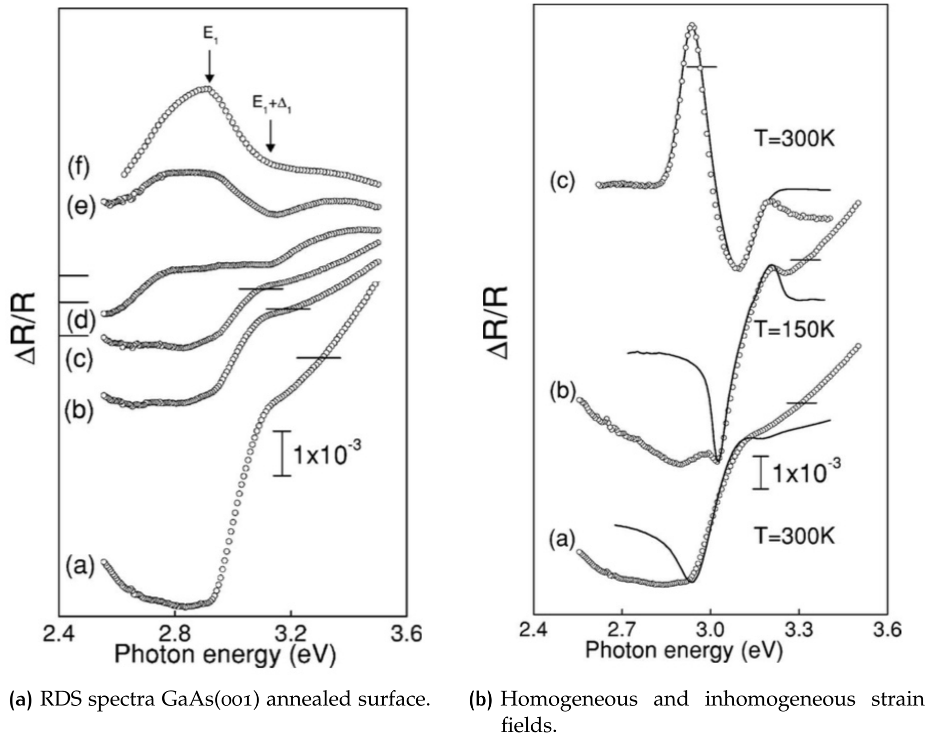

(a) RDS spectra GaAs(001) annealed surface.

(b) Homogeneous and inhomogeneous strain fields.

Figure 24: Left: Sequence of RD spectra of the GaAs 001 surface re- constructions obtained by thermal desorption. Right: Spectrum (a) of left figure where (hollow circles) and its theoretical line shape (solid lines) were obtained by 2D line shapes. RD spectra taken from literature [38] for [1$\bar{1}$0] uniaxial applied stress (hollow circles) and its theoretical model (solid lines) obtained by using excitonic line shapes.Spectra taken from literature ref. [29]

mechanism that ionizes excitons near the surface is temperature independent [29].

By analyzing the evolution of these spectra with the surface geometry, they isolated the RD component associated with the surface strain induced by the reconstruction. In order to fit the measured RD spectra, they used the line shape for the bulk strain component while considering that near the surface the strain is inhomogeneous along the direction perpendicular to the surface and that the strain-induced electric field ionizes the excitons, thus quenching the excitonic effect that is present in the bulk of semiconductor samples [29].

The fitting of the experimental RD spectrum of Fig.24b reproduces well the experimental spectrum, thus supporting the assumption about its surface-strain origin.

3 EXPERIMENTAL RESULTS

3.1 INAS SAMPLE AND EXPERIMENTAL SETUP PREPARATION

This chapter focuses on the description and results of the experimental growth of heteroepitaxial semiconductor structures, in specific, InAs. As was stated in the previous chapter, self-assembled quantum dots integrated into semiconductor heterostructures, are highly attractive for device application due to their discrete energy levels and optical properties. In particular, QD's computers, QD lasers and infrared photodetectors are some of the devices where InAs QD's are applied [45],[46].

In every case, epitaxial growth was carried out in a solid source MBE chamber, on semi-insulating GaAs (001) substrates, where the only variables are the substrate's temperature and the As overpressure. As was described in the first chapter, a valved As cell allowed the control of As flux which varies in some cases. The growth rate of InAs was determined through a comparison of RHEED oscillation periods of GaAs and $In_{0.3}Ga_{0.7}As$ films grown on GaAs. In every case, prior to InAs growth, a GaAs buffer layer was grown at a temperature of 600°C. Then the substrate temperature was lowered until the desired temperature was reached, thus allowing enough time for the surface reconstruction to stabilize in a c(4x4) RHEED pattern. Once the surface stabilization is reached, InAs growth started by opening the In shutter. The growth then is interrupted by closing the In shutter after deposition of the desired InAs equivalent monolayers.

Although the spectral range differ somehow in the measurements with both spectrometers, both comprised GaAs and InAs E_1 and $E_1+\Delta_1$ energy transitions. The experimental set up allowed for the simultaneous measurement of RD spectra and observation of RHEED diffraction patterns in order to establish a correlation between the surface reconstruction and RD line shape along the whole epitaxial growth period.

3.2 HETEROEPITAXIAL GROWTH; RDS MEASUREMENTS WITH A 32-CHANNEL LOCK-IN

This set of experiments was carried out using the RD spectrometer with a 32-channel Lock-In adapted for data acquisiton (see chapter 1) in the range that comprises 330nm to 680 nm (3.8-1.9 eV). RD spectra were acquired at a rate of 10 spectra per second. The same As overpressure, P = $5x10^{-6}$ Torr, was implemented in all the experiments, but different substrate temperatures, 460°C and 480°C. In both cases, RDS spectra and RHEED patterns were measured at the mu-

tually orthogonal crystallographic directions, [110] as well as [1$\bar{1}$0].

3.2.1 InAs/GaAs(001) growth at T=480°C

In this particular experiment, an equivalent of 4 monolayeres of InAs were grown at a substrate temperature of 480°C. RDS measurements and RHEED diffraction patterns were measured in both crystallographic directions, [110] and [1$\bar{1}$0], and the results are presented for comparision.

3.2.1.1 *RDS and RHEED measurements along* [110]

With filled circles, in Fig.25a, are shown selected, time-resolved RD spectra acquired during the growth of InAs/GaAs QD's. Spectra in such figure, are vertically displaced for the sake of clarity. Zeros for each spectrum are indicated by horizontal black bars. Continuous lines in Fig.25a correspond to spectra fits as discussed below. Spectrum a) in Fig.25a was measured just before starting growth. It shows the typical line shape for a c(4x4) surface reconstruction with a minimum close to the GaAs E_1 interband energy transition [47]. Spectra b)-e) were measured at various times during growth as indicated, with t=0 corresponding to growth onset. Spectrum f) was measured at the end of the experiment, with about 4 ML of InAs being deposited on the GaAs substrate.

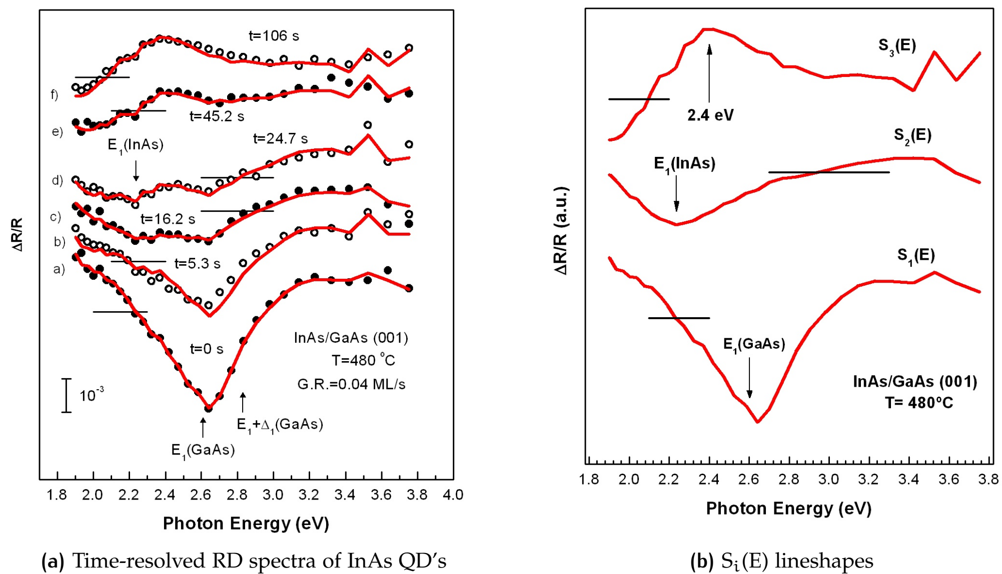

(a) Time-resolved RD spectra of InAs QD's

(b) $S_i(E)$ lineshapes

Figure 25: InAs/GaAs growth selected time-resolved RD spectra and the $S_i(E)$ lineshapes derived from an SVD analysis of such spectra.

Upon starting growth, the amplitude of the initial RD spectrum gradually decreases and eventually vanishes. At the same time, as spectra c)-d) show, a spectral feature develops cen-

tered around 2.23 eV, which is close to the InAs E_1 transition.This feature eventually disappears as growth progresses, thus corresponding to an intermediate stage in the quantum dot growth. At the end of the growth, once quantum dots are fully grown as shown by RHEED patterns, the RD spectrum changes sign with respect to the initial c(4x4) spectrum and shifts to lower energy for about 0.21 eV. Visual inspection of Fig.25a strongly suggests that time-dependent RD spectra comprise more than one independent spectral component as SVD analysis technique described previously, suggests.

A first spectral component, which will be denoted as $S_1(E)$, is given by the initial c(4x4) spectrum. As was previously reported, this spectrum is to a large extent due to the orthorhombic strain induced by surface reconstruction [36]. A second one, denoted as $S_3(E)$, is provided by the spectrum at the end of the run (t=106 s) which corresponds to fully formed QD's. Such spectrum, which arises from a surface with 3D features as its RHEED pattern indicates, show a spectral signature similar to that of the first component, but displaced downwards in energy for about 0.21 eV. The final $S_3(E)$ spectrum is at least partially associated to the InGaAs QD's which are presumably anisotropically strained by either the preferential generation of α-type misfit dislocations or by the elastic interaction of anisotropic QD's with the GaAs surface. Regarding the first mechanism, it is known that for (001) interfaces misfit dislocations are preferentially generated with cores along [110], thus leading to overlayers or QD's with orthorhombic symmetry. Alternatively, an orthorhombic symmetry may result from the z-dependent elastic relaxation of the interface strain in quantum dots with in-plane asymmetric shape. In such a case, the sign of the anisotropy spectrum will depend on QD's morphology, i.e., the direction, either $[1\bar{1}0]$ or [110] along which their dimensions are larger. We further note that the InAs wetting layer may as well contribute to the final spectrum, with a component that could overlap in energy with $S_3(E)$ [48],[49]. Finally, the third spectral intermediate component, denoted as $S_2(E)$, was obtained from a linear combination of experimental spectra. In Fig.25b we show the three basic line shapes obtained as outlined above. Spectra in Fig.25b have been vertically displaced in the sake of clarity. Zeros for each spectrum are indicated by horizontal black bars. We note that component $S_2(E)$ shows similar features to those of component $S_1(E)$, although it is centered around the InAs E_1 interband transition rather than around that of GaAs. This suggests that component $S_2(E)$ is originated from InAs-rich islands or from an InAs wetting layer existing before forming QD's.

Continuous lines in Fig.25a show fittings to selected RD spectra. As it can be seen, they accurately reproduce all essential features of experimental spectra as required. Fig.26 show $c_i(t)$ coefficients as a function of time during the whole epitaxial growth. Fig.26a shows the time evolution of coefficient $c_1(t)$ which corresponds to the initial c(4x4) spectrum. As expected, coefficient $c_1(t)$ decreases monotonically upon starting growth as InAs surface coverage gradually increases. On the basis of growth rate, full InAs surface coverage should be reached at about t=25 s. According to Fig 25a, nevertheless, it takes longer for the initial RD spectrum to disappear, thus indicating that epitaxial growth did not proceed in a full layer-by-layer mode and supporting the suggestion that line shape $S_2(E)$ originates in InAs-rich islands.

Figs. 26 b and c also show the time evolution of coefficients $c_2(t)$ and $c_3(t)$. Coefficient $c_3(t)$ describes the formation of InGaAs quantum dots and gradually increases upon starting growth and saturates after about 50 s, which corresponds to 2 ML InAs growth. In contrast, coefficient $c_2(t)$ first increases, reaches a maximum at about 1 ML and then decreases to become

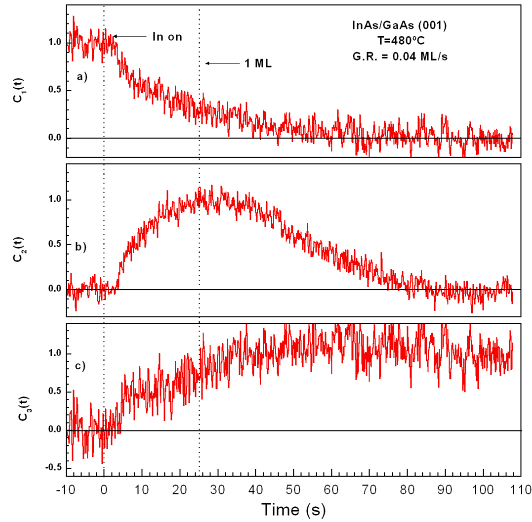

Figure 26: Time evolution of the three components that comprise the time-dependent RD spectra measured during the epitaxial growth of InAs/GaAs.

zero at a time about t= 80 s.This indicates that $c_2(t)$ corresponds to a precursor stage in the formation of quantum dots which would be mediated by the nucleation of InAs-rich islands that eventually merge into InGaAs quantum dots.

RDS analysis is backed up by taking a look at RHEED patterns and oscillations. In Fig.27 the diffraction patterns show the evolution of InAs surface as time passes. The complete evolution from Fig.27a to Fig.27e, covers a surface change from a GaAs c(4x4) to 1 ML of deposited InAs (see Fig.27d), which transforms the surface to a (1x) reconstruction, giving then, place to some kind of 1/2 ordered surface, but with weak surface reconstruction lines (see Fig.27e), a complete spotted diffraction pattern is seen in Fig.27e after In shutter has been opened for about 106s, this pattern is related to self assembled quantum dots.

Analyzing Fig.28 a minimum at about 25 s corresponds to the deposition of 1 ML of InAs, if a layer by layer deposition took place, at the same time it is well known RHEED that a minimum in the oscillation corresponds to a rough surface, though the next minimum does not reach the same initial point as the first one quenching the attempts of another InAs monolayer to form, which agrees with a Stransky-Krastanov growth mode.

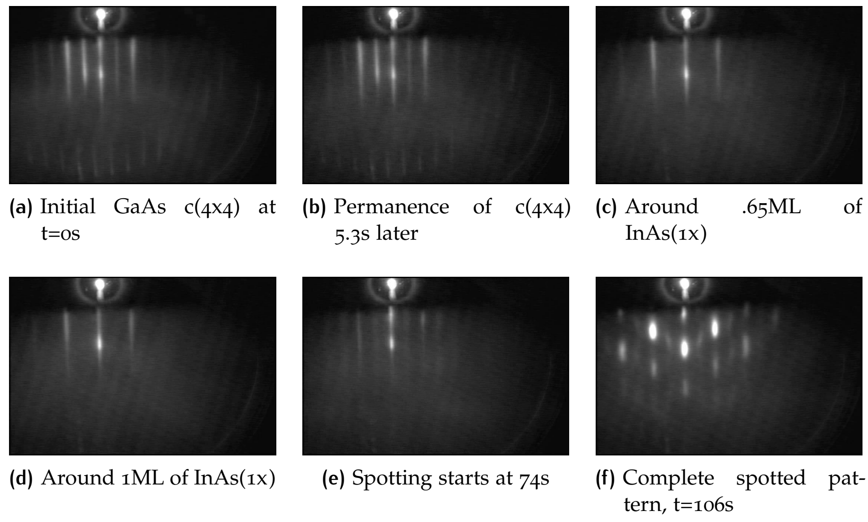

(a) Initial GaAs c(4x4) at t=0s
(b) Permanence of c(4x4) 5.3s later
(c) Around .65ML of InAs(1x)
(d) Around 1ML of InAs(1x)
(e) Spotting starts at 74s
(f) Complete spotted pattern, t=106s

Figure 27: Selected RHEED patterns along [110] of InAs/GaAs (001).

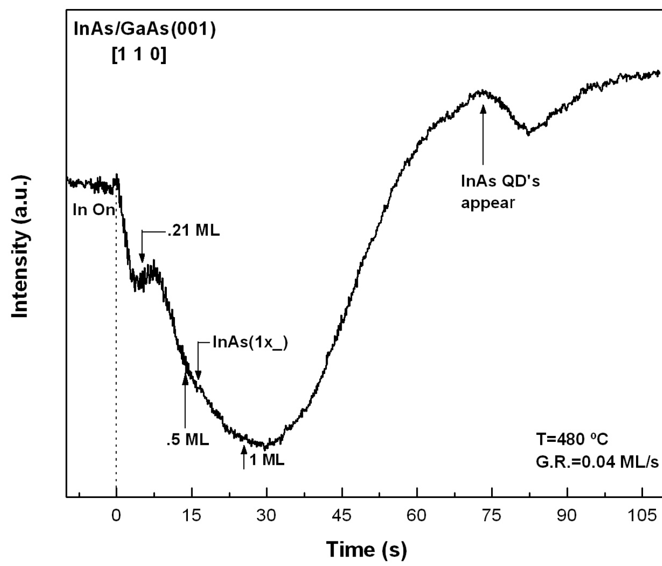

Figure 28: RHEED measured oscillations along [110] of InAs/GaAs (001) growth.

3.2.1.2 *RDS and RHEED measurements along* $[1\bar{1}0]$

After the deposition of InAs/GaAs(001) during which the observation of RHEED diffraction patterns and oscillations of bulk (00) along [110] crystallographic direction were measured, the substrate's temperature was raised until 600° C were reached in order to start the desorption of In from the surface and obtain the well known GaAs (2x4) surface reconstruction. After the In desorption, the surface was impinged by Ga and As flux so that the GaAs (2x4) surface reconstruction might be reached faster and remaining In atoms could be covered by a thin GaAs overlayer. Then, the temperature was lowered again until a 480° C temperature was reached and a c(4x4) GaAs surface reconstruction was visible in the RHEED diffraction patterns. Once time passed by allowing the stabilization of the c(4x4) GaAs surface, the substrate was rotated in order to measure RHEED oscillations (and diffraction patterns) along the $[1\bar{1}0]$ crystallographic direction. RD spectra were measured at unison so any anisotropic variation during the surface growth would be shown in its analysis. In Fig.29a and with filled circles, are shown some selected time-resolved RD spectra acquired during the growth of InAs/GaAs QD's, whereas continuous lines correspond to spectra fits. Spectrum a) in Fig.29a was measured just before starting growth. It shows the typical line shape for a c(4x4) surface reconstruction with a minimum close to the GaAs E_1 interband energy transition [47]. Spectra b)-e) were measured at various times during growth as indicated, with t=0 corresponding to growth onset. Spectrum f) was measured at the end of the experiment, wich corresponds to about 6 ML of InAs deposited on the GaAs substrate.

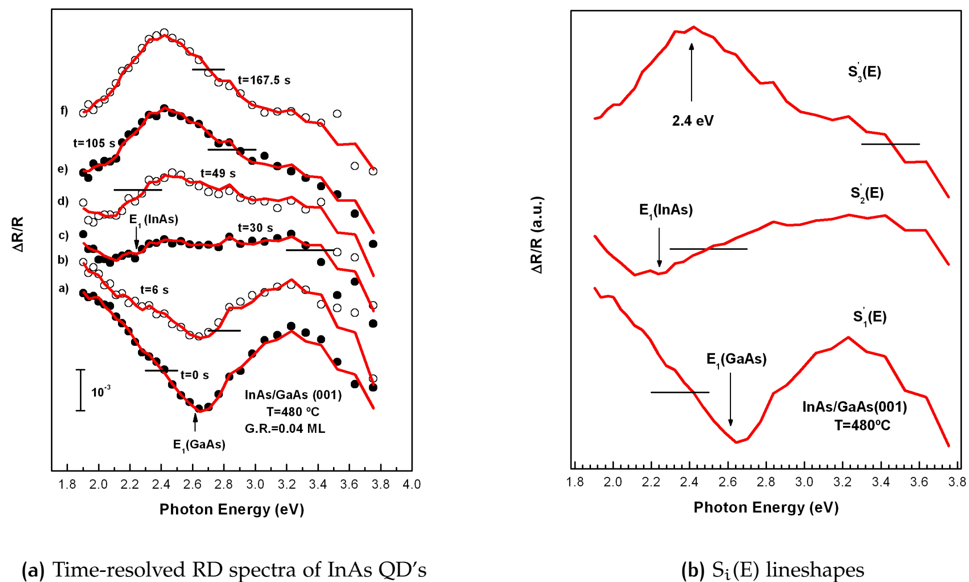

(a) Time-resolved RD spectra of InAs QD's

(b) $S_i(E)$ lineshapes

Figure 29: InAs/GaAs growth selected time-resolved RD spectra and the $S'_i(E)$ lineshapes derived from an SVD analysis of such spectra.

Upon starting the growth the amplitude of the initial RD spectrum gradually decreases and eventually vanishes. At the same time, as spectra c)-e) show, a distinctive spectral feature develops centered around 2.23 eV, which is close to the InAs E_1 transition. This feature eventually disappears as growth progresses, thus corresponding to an intermediate stage in the quantum dot growth. At the end of the growth, once quantum dots are fully grown as can be seen in the RHEED diffraction patterns taken during the growth (see Fig.31), the RD spectrum changes sign with respect to the initial c(4x4) spectrum and has a redshift towards 0.23 eV. Visual inspection of Fig.29a also suggests that time-dependent RD spectra comprise of three independent spectral component as well as in the previous experiment.

The first espectral component, denoted as $S'_1(E)$, is given by the initial c(4x4) spectrum. A second one, denoted as $S'_3(E)$, is provided by the spectrum at the end of the experiment (t=167.5 s) which corresponds to fully formed QD's, as its RHEED pattern indicates. Finally, the third spectral intermediate component, denoted as $S'_2(E)$, was obtained from a linear combination of two SVD spectral components. In Fig.29b are shown the three basic line shapes obtained as described before. As in the measurements taken along the [110] crystallographic direction, the component $S'_2(E)$ shows similar features to those of component $S'_1(E)$, but centered around InAs E_1 interband transition instead than that of GaAs, reinsuring that it was related either to the InAs islands or to the existence of the wetting layer.

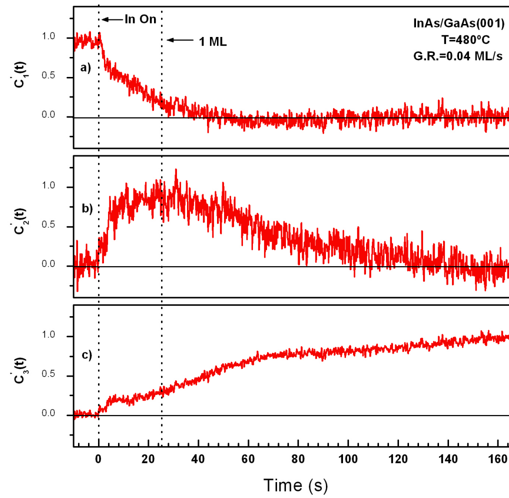

Figure 30: Time evolution of the three components that comprise the time-dependent RD spectra measured during the epitaxial growth of InAs/GaAs.

As well as in the previous measurements, Fig.29a show accurate fittings to the selected RD experimental spectra. Fig.30 show $c'_i(t)$ coefficients as a function of time during the whole epitaxial growth. Fig. 30a shows the time evolution of coefficient $c'_1(t)$ which corresponds to the initial GaAs c(4x4) spectrum. As expected, coefficient $c'_1(t)$ decreases monotonically upon starting growth as InAs surface coverage gradually increases. On the basis of growth rate, full InAs surface coverage should be reached at about t=25 s. According to Fig.29a, around 30 s

after deposition started (see spectrum (c)) the GaAs characteristic minimum around E_1 critical point has already disappeared giving place to a maximum and a slightly displacement towards low energies. Eventhough not shown in this work, the corresponding spectrum measured at this point (t=25 s), has also suffered this sign change from negative to positive and displacing of .2 eV, from around 2.6 towards 2.4 eV, showing a similar structure to that of spectrum (c) in Fig.29a.

Figs.30 b and c show the time evolution of coefficients $c'_2(t)$ and $c'_3(t)$, respectively. Coefficient $c'_3(t)$ describes the disappearance of the GaAs c(4x4) surface reconstruction (shown by the bump seen around 5 s after being opened the In shutter), giving place to the (1x3) InAs surface reconstruction (as seen in Fig.31 and as described in reference [25]) and indicating eventually the appearance of InGaAs quantum dots around 70s. This $c'_3(t)$ lineshape increases gradually upon starting growth and appeared to saturate around 90 s (around 3.6 ML), but continues to augment as the InGaAs quantum dots grow in size though not in density (see reference [26] or subsection 2.4.1 for a more detailed explanation). In contrast, coefficient $c'_2(t)$ first increases and reaches its maximum at about 1 ML and then decreases to become zero at a time about t= 100 s.This indicates that $c'_2(t)$ corresponds to a precursor stage in the formation of quantum dots or InAs wetting layer, as was also shown in the analogous experiment measured along [110].

In Fig.31 the diffraction patterns show the evolution of InAs surface through time. The evolution from Fig. 31a to Fig.31c, covers a surface change from a GaAs c(4x4) to a (x3) reconstruction and about 1 ML of InAs. Then, the reconstruction lines disappear giving place to a spotted diffraction pattern with chevron-like shaped dots, as is seen in Fig.31d. After In shutter has been opened for about 105s, this pattern increases the chevrons intensity.

As the growth rate, continues to be of .04 ML/s, around 25 s, there should be 1 ML of InAs as in the prior case, though the minimum of the oscillation is not exactly at 25 s, being instead positioned around 40 s as can be seen in Fig.32. Eventhough the ocurrence of the chevrons match in time with the ocurrence of the spotted diffraction pattern seen along the [110] crystallographic direction, it can be seen in the RHEED oscillations of both experiments that along [110] the diffraction patterns appear at the maximum of the oscillation (see Fig.28), whereas the chevron diffraction pattern along [$1\bar{1}0$], occurs along the positive slope between the maximum and the minimum of its oscillation (see Fig.32).

Another observation to recall from both, Fig.28 and Fig. 32 is the similar behavior the RHEED oscillations present in comparison to the ones in [26]. Although both of the oscillations have the changes in slope presented in reference [26], the QD's along [110] appeared in the second slope region and the chevrons along [$1\bar{1}0$] appeared in the first slope region, suggesting that the QD's formed during the first experiment might not be sufficiently big to diffract (in average) the electrons towards the photoluminiscence screen direction until they grow enough, i.e. when the second slope is observed in the RHEED oscillation. On the other hand, the chevrons are sharper and therefore it is assumed that in the second experiment, the quantum dots are big enough, at least along that crystallographic direction, to be seen in the oscillation even before the second slope is reached.

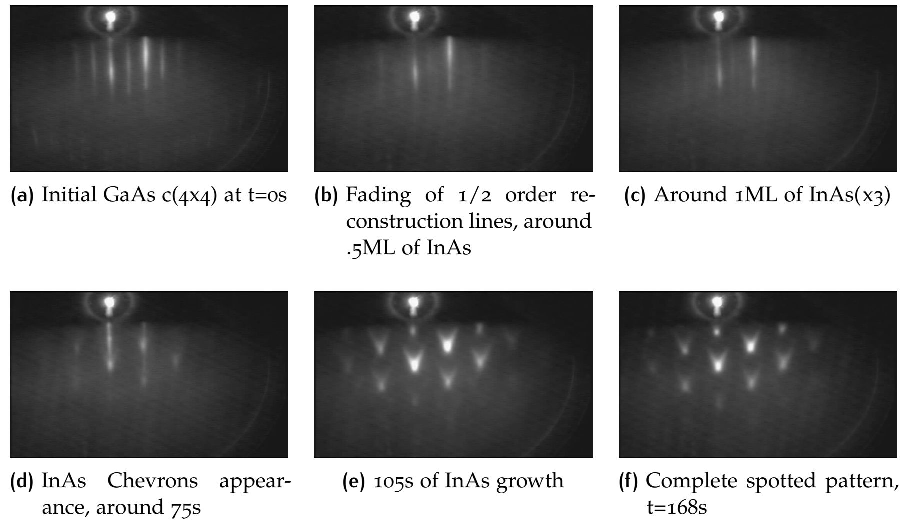

(a) Initial GaAs c(4x4) at t=0s

(b) Fading of 1/2 order reconstruction lines, around .5ML of InAs

(c) Around 1ML of InAs(x3)

(d) InAs Chevrons appearance, around 75s

(e) 105s of InAs growth

(f) Complete spotted pattern, t=168s

Figure 31: Selected RHEED patterns along [1$\bar{1}$0] of InAs/GaAs (001).

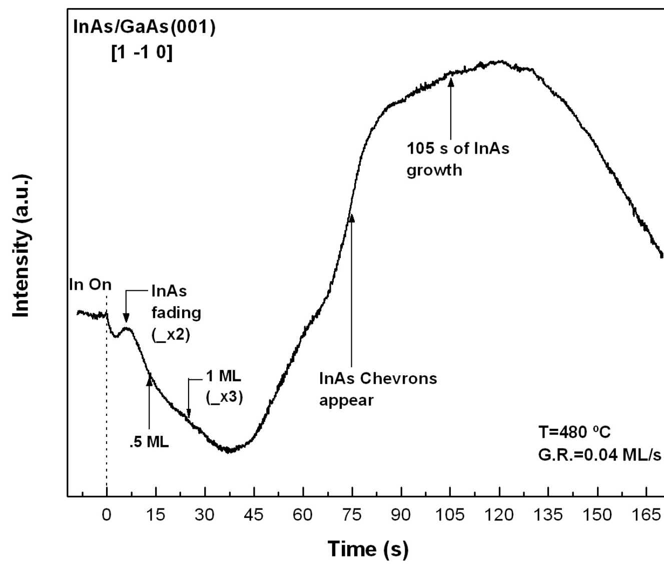

Figure 32: RHEED oscillations measured along [1$\bar{1}$0] of InAs/GaAs (001) growth.

3.2.2 InAs/GaAs(001) growth at T=460°C

In this experiment, an equivalent of 5 monolayeres of InAs were grown at a substrate temperature of 460°C. RDS measurements and RHEED diffraction patterns were measured in both crystallographic directions, [110] and [1$\bar{1}$0], and the results are presented for comparision with those measured at 480°C

3.2.2.1 *RDS and RHEED measurements along* [110]

Figure 33, shows a set of selected time-resolved RD spectra acquired during the growth of InAs/GaAs QD's, as well as the $S''_i(E)$ lineshapes derived from SVD and further analysis. Spectra in this figure, are also vertically displaced in the sake of clarity and as well, the zeros are indicated by horizontal black bars. Continuous lines in Fig.33a correspond to the spectral fits; Spectrum a) in Fig.33a was measured just before starting the growth, it also corresponds to the line shape of a GaAs c(4x4) surface reconstruction. Spectra b)-e) correspond to the evolution of the anisotropies in time as they were measured at various times during growth, time t=0 corresponds to the growth onset. Spectrum f) was measured at the end of the experiment, with about 5 ML of InAs deposited over the GaAs substrate.

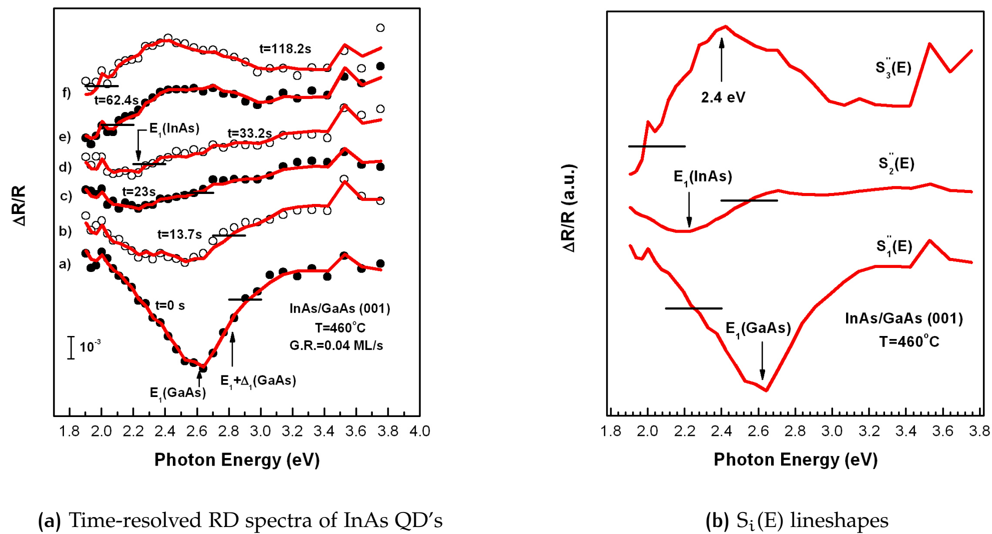

(a) Time-resolved RD spectra of InAs QD's

(b) $S_i(E)$ lineshapes

Figure 33: InAs/GaAs growth selected time-resolved RD spectra and the $S_i(E)$ lineshapes derived from an SVD analysis of such spectra.

Having lowered the temperature of the substrate by only 20°C, it is expected to start the growth at the same initial c(4x4) surface reconstruction as was proved by both, RDS and RHEED measurements. As well, the behaviour in the RDS spectra continues to be very similar to those of the previous experiments, the amplitude of the initial RD spectrum gradually decreases and eventually vanishes. The same spectral feature developed around 2.23 eV, i.e. InAs

E_1 transition, still appears in this series of spectra, though it is somehow more subtle than in the case of InAs growth at 480°C. But, it eventually disappears as well. As same as in previous experiments, at the end of the growth, RD spectrum still changes its sign with respect to the initial c(4x4) spectrum and shifts to lower energy for about 0.23 eV. Doing the same analysis as before, it has been found that the same spectral components are needed to shape each of the experimental spectrum as it is seen in Fig 33b.

The first spectral component, $S''_1(E)$, is given by the initial c(4x4) spectrum. The second one, denoted as $S''_3(E)$, is provided by the spectrum at the end of the run (t=130 s) which corresponds to fully formed QD's. Such spectrum, which arises from a surface with 3D features as its RHEED pattern indicates, shows a spectral signature similar to that of the first component, but displaced downwards in energy for about 0.23 eV. The final $S''_3(E)$ spectrum is associated to the InGaAs QD's, as suggested before, the InAs wetting layer may as well contribute to the final spectrum. Finally, the third spectral intermediate component, denoted as $S''_2(E)$, in this case, was obtained directly from SVD analysis. In Fig.33b the three basic line shapes obtained as outlined above, are shown. From the last two experiments, as well as from this, it is noted that the spectral component $S''_2(E)$ shows similar features to those of component $S''_1(E)$, although centered around the InAs E_1 interband transition rather than around that of GaAs. This suggests that component $S''_2(E)$ is originated from small InAs-rich islands or from an InAs wetting layer existing before forming QD's.

Continuous lines in Fig.33a show fittings to selected RD spectra. As it can be seen, they accurately reproduce all essential features of experimental spectra as required. In Fig.34, the function of time $c''_i(t)$, $S''_1(E)$ coefficients, are shown as the evolution of each spectral component during the whole epitaxial growth. Fig.34a shows the time evolution of coefficient $c''_1(t)$ which corresponds to the initial c(4x4) spectrum. As expected, coefficient $c''_1(t)$ decreases monotonically upon starting growth as InAs surface coverage gradually increases. On the basis of growth rate, full InAs surface coverage should be reached at about t=25 s. According to Fig.33a, it takes about that time for the initial RD spectrum to disappear, although this not corresponds exactly to previous experiments, it is still believed that the epitaxial growth did not proceed in a full layer-by-layer mode due to the maximum reach of $S''_2(E)$'s coefficient line shape, $c''_2(t)$ which somehow indicates the evolution in time of the InAs E_1 interband transition, which suggests that during this InAs 1 ML deposition, InAs-rich islands are grown at the same time as the wetting layer.

In Fig.35 the diffraction patterns show the evolution in time of GaAs c(4x4) surface as it is being covered by InAs. The evolution from Fig.35a to Fig.35c, covers a surface change from a GaAs c(4x4) to a (1x) reconstruction and about 1 ML of InAs. Then, the reconstruction lines disappear giving place to some kind of faded (2x) reconstruction lines (see Fig.35d) which then starts to cover gradually with a spotted diffraction pattern (see Fig.35e) until both, bulk and reconstruction lines are completely covered with diffraction spots as seen in Fig.35f.

The oscillation minimum is still around 1 ML of InAs as in the prior case, as can be seen in Fig.36. The ocurrence of the InAs diffraction spots happens around the maximum of the RHEED oscillation (at about 75s after the growth started) as it happened in the experiment measured at 480°C which can be corroborated looking at Fig.28.This particular moment, also corresponds to the time where coefficient $c''_3(t)$ saturates mantaining an almost zero slope

(see Fig.34c). Also, in this evolution, the characteristic bump around 12 s shows the change in surface reconstruction from the well known GaAs c(4x4) to the also known InAs (1x3), which also agrees with the diffraction patterns and RHEED oscillation shown in figures Fig.35 and Fig.36, respectively.

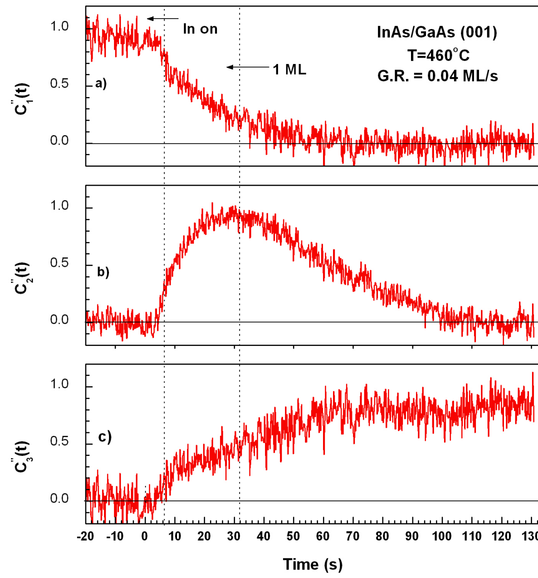

Figure 34: Time evolution of the three components that comprise the time-dependent RD spectra measured during the epitaxial growth of InAs/GaAs.

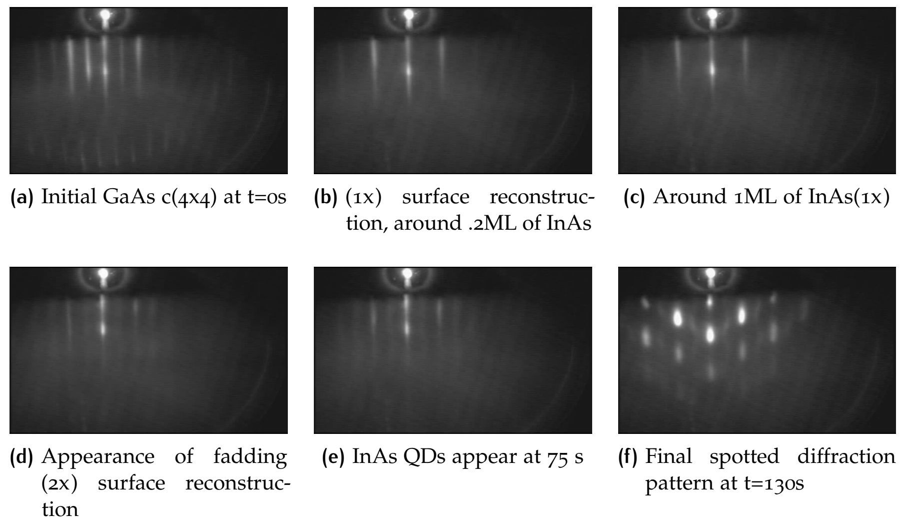

(a) Initial GaAs c(4x4) at t=0s

(b) (1x) surface reconstruction, around .2ML of InAs

(c) Around 1ML of InAs(1x)

(d) Appearance of fadding (2x) surface reconstruction

(e) InAs QDs appear at 75 s

(f) Final spotted diffraction pattern at t=130s

Figure 35: Selected RHEED patterns along [110] of InAs/GaAs (001).

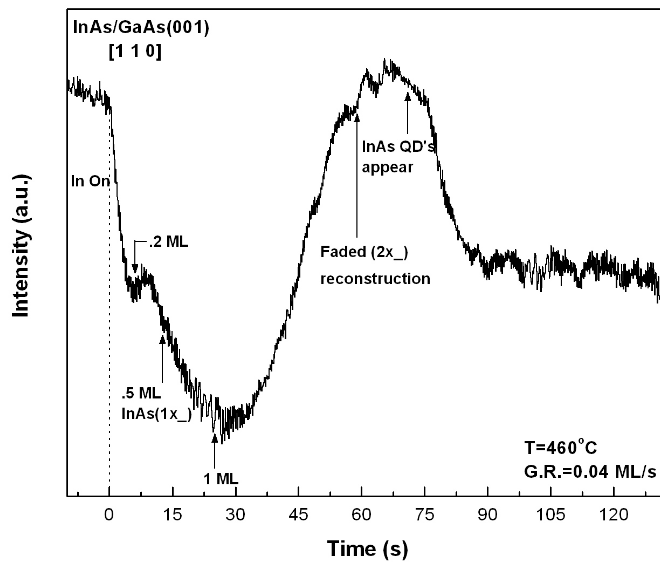

Figure 36: RHEED oscillations measured along [110] of InAs/GaAs (001) growth.

3.2.2.2 *RDS and RHEED measurements along* [1$\bar{1}$0]

Fig.37 shows a set of selected time-resolved RD spectra acquired during the growth of InAs/-GaAs QD's as well as the $S'''_i(E)$ lineshapes derived with the help of SVD analysis. Spectra in this figure, are vertically displaced in the sake of clarity and as well, the zeros for each spectrum are indicated by horizontal black bars. Continuous lines in Fig.37a correspond to the spectra fits discussed ahead; Spectrum a) in Fig.37a was measured before starting the growth, it corresponds to the line shape of a GaAs c(4x4) surface reconstruction. Spectra b)-e) correspond to the evolution of the anisotropies as the growth was taking place. Spectrum f) was measured at the end of the experiment, with about 8 ML of InAs deposited over the GaAs substrate.

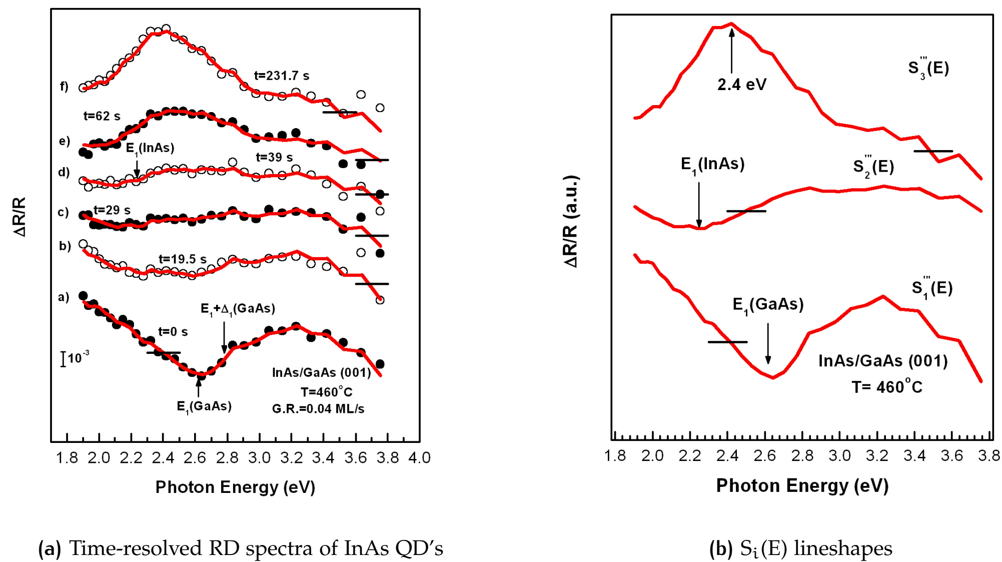

(a) Time-resolved RD spectra of InAs QD's

(b) $S_i(E)$ lineshapes

Figure 37: InAs/GaAs growth selected time-resolved RD spectra and the $S'''_i(E)$ lineshapes derived from an SVD analysis of such spectra.

RDS spectra continues to be very similar to those of its analogous experiment at 480°C, the amplitude of the initial RD spectrum gradually decreases giving place to a spectrum with this distinctive feature around 2.23 eV, which corresponds to InAs E_1 transition. Even though it is somehow more subtle than in the case of InAs growth at 480°C. Then, this spectrum evolves too, changing its sign with respect to the initial c(4x4) spectrum and shifts to lower energies for about 0.25 eV. Doing the same analysis as in the previous 3 experiments, it has been found that the same spectral components are needed to shape each of the experimental spectrum as it's seen in Fig 37b.

The spectral components, seem pretty similar to those of the experiment grown at 480°C, $S'''_1(E)$, represents the initial c(4x4) spectrum. $S'''_3(E)$, is provided by the spectrum at the end of the run (t=231.7 s) and due to its shape and position of its critical points, it's still associated

to the InGaAs QD's and the wetting layer grown before. Finally, the third spectral intermediate component, denoted as $S'''_2(E)$, was in this case, also obtained directly from SVD analysis. In Fig.37b are shown the three basic line shapes obtained as outlined above. The same as in previous cases, component $S'''_2(E)$ shows similar features to those of component $S'''_1(E)$, although it is centered around the InAs E_1 interband transition rather than around that of GaAs, which confirms the origins of component $S'''_2(E)$ are those defined for its analogous experiment, small InAs QD's or/and its wetting layer formation.

Continuous lines in Fig.37a show fittings to selected RD spectra and they accurately reproduce all essential features of experimental spectra as required. How the spectral components combine themselves to reproduce those experimental spectra is described by the evolution in time of each of the corresponding coefficients of each spectral component, this can be appreciated in Fig.38 as it shows the time evolution of this coefficients. Fig.38a shows the coefficient corresponding to the evolution of the initial c(4x4) spectral component $S'''_1(E)$, as expected, coefficient $c'''_1(t)$ decreases monotonically upon starting growth of InAs and it covers the surface gradually. On the basis of growth rate, full InAs surface coverage should be reached at about t=25 s. According to Fig 38a, it takes a little bit longer for the initial RD spectrum to disappear, about 38s, which suggests that the epitaxial growth wasn't in a full layer-by-layer mode. In Fig.38c can be seen the now characteristic bump that is also seen in some kinetical RDS studies (see reference [25]) made around 2.5 eV and that corresponds to the vanishing of the GaAs c(4x4) surface to give place to that InAs well known (1x3) surface reconstruction. When this bump disappears, around 25 s, it also corresponds to the maximum seen in Fig.38b, coefficient that its related to the coverage on GaAs surface by InAs, partially by the wetting layer and partially by small InAs QD's as can also be referred too in [5].

In Fig.39 the diffraction patterns show the evolution of InAs surface through time. The evolution from Fig.39a to Fig.39c, covers a surface change from a GaAs c(4x4) to a (x3) reconstruction and about 1 ML of InAs. Then, the reconstruction lines disappear giving place to a chevron-like diffraction pattern (see Fig.39e to Fig.39f) which enhances its intensity while the surface is being covered until the end of the experiment, where the intensity seems to have diminished.

The oscillation minimum is beyond the mark of 1 ML's InAs deposition, as well as in the case of growth at 480°C, see Fig.40. The appearance of the InAs diffraction spots starts before the maximum (at about 75s after the growth started) of RHEED's oscillation is reached, but as stated before, they are at its maximum intensity after 112 s have passed since the growth started.

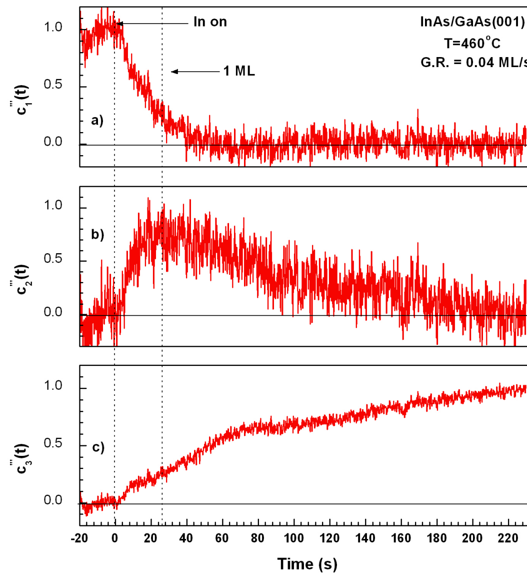

Figure 38: Time evolution of the three components that comprise the time-dependent RD spectra measured during the epitaxial growth of InAs/GaAs.

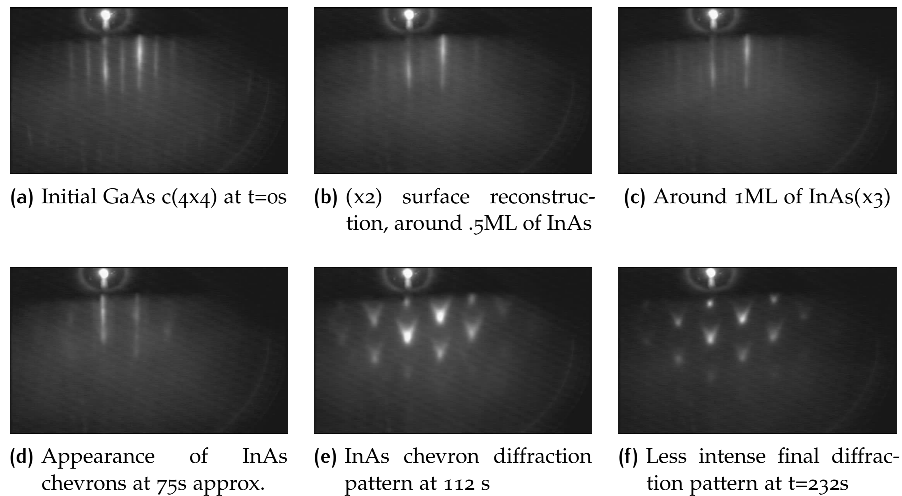

(a) Initial GaAs c(4x4) at t=0s

(b) (x2) surface reconstruction, around .5ML of InAs

(c) Around 1ML of InAs(x3)

(d) Appearance of InAs chevrons at 75s approx.

(e) InAs chevron diffraction pattern at 112 s

(f) Less intense final diffraction pattern at t=232s

Figure 39: Selected RHEED patterns along $[1\bar{1}0]$ of InAs/GaAs (001).

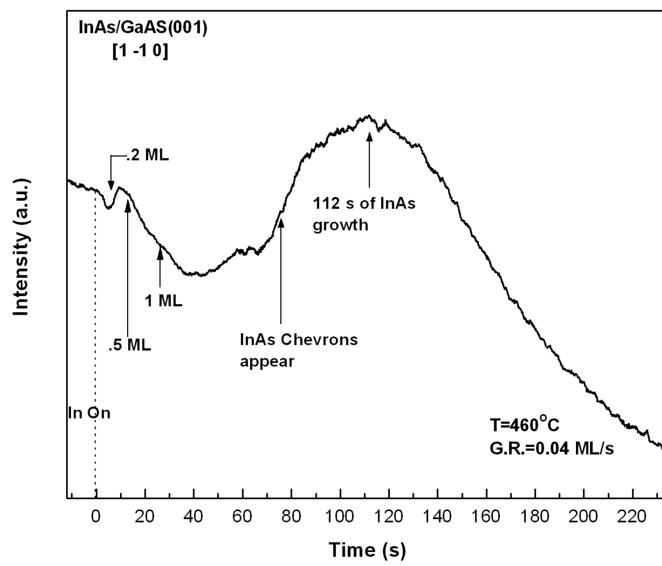

Figure 40: RHEED oscillations measured along $[1\bar{1}0]$ of InAs/GaAs (001) growth.

3.2.3 Defining S_1 and S_2 as strain bases

Following the identification of the bases used to comprise all the RDs lineshapes in the previously presented experimental results, the modeling of those lineshapes with the physical phenomena of strain, described in subsection 2, is the most accurate model which will describe the generalities of the evolution of the InAs/GaAs(001) surface. In the following figures an excitonic strain fit is presented of each of the S_1 bases obtained by the SVD analysis.

Eventhought an excitonic lineshape isn't expected at such high temperatures, based in Lautenschlager (see reference [33]) work, at high temperatures the GaAs exciton hasn't completely disappeared, it can be explained as a combination of remaining GaAs excitons along with continuum interband transitions corresponding to a 2D lineshape.

As well as S_1 is fitted by this strain model before the growth starts and along its whole evolution, a component of GaAs strain represented by such lineshape, is always present during the growth, diminishing during InAs deposition and augmentating the corresponding InAs strain component. S_1 is being modeled in the following figures 41 and 42 at 480° C and at 460° C, respectively.

In the S_1 lineshape obtained from the measured spectra along the $[1\bar{1}0]$ crystallographic axis (seen in 41 and 42), around high energies, it can be seen that there's a shoulder in comparison to the corresponding S_1 lineshape obtained from the measured spectra along the $[110]$ axis, this might be due to some inaccuracies during the rotation of the sample before the growth.

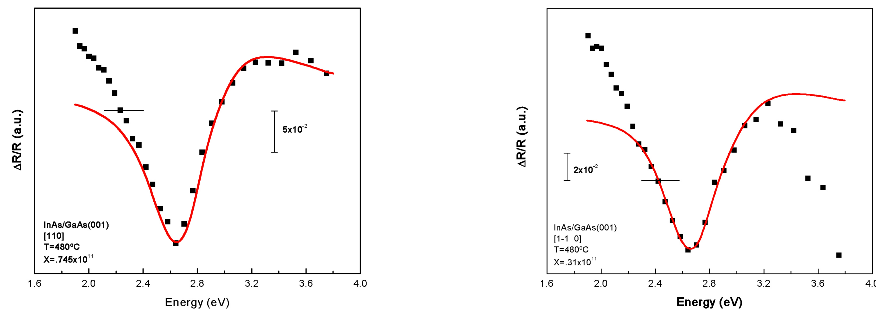

(a) Strain fit, S_1 lineshape obtained from RDS exp data

(b) Strain fit, S_1 lineshape obtained from RDS by rotating the sample $\pi/2$

Figure 41: The SVD obtained S_1 lineshapes for the 480°C InAs growth, along both crystallographic directions are shown in the figures (depicted in closed circles), as well as their strain fit (seen in red as a solid lineshape)

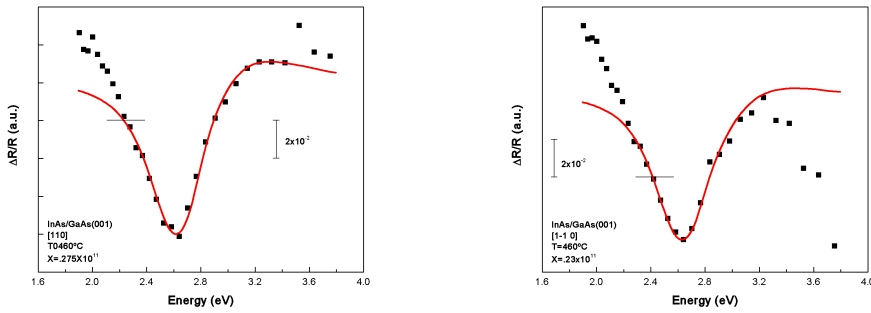

(a) Strain fit, S_1 lineshape obtained from RDS exp data

(b) Strain fit, S_1 lineshape obtained from RDS by rotating the sample $\pi/2$

Figure 42: The SVD obtained S_1 lineshapes for the 460°C InAs growth, along both crystallographic directions are shown in the figures (depicted in closed circles), as well as their strain fit (seen in red as a solid lineshape)

3.3 HETEROEPITAXIAL GROWTH; RDS MEASUREMENTS WITH A 2-CHANNEL LOCK-IN

This set of experiments were carried out using the RD spectrometer with a 2-channel Lock-In adapted for data acquisiton (see chapter 1) in the spectral range of (356-581) nm. Due to the way of acquiring data, this spectra have a considerable noisy background (see Fig.43) and so do their respective fits. Nevertheless it was important to add them to the analysis due to the information that can be extracted in terms of the changes in the spectral components owed to the changes in As pressure. RD spectra were acquired at a rate of 1 spectrum per .333 seconds. The same substrate temperature of T=480°C was implemented in each one of the experiments, but different As overpressures in each of the measurements, being them P_1 = 5x10^{-6} Torr, P_2 = 2x10^{-6} Torr, and P_3 = 6x10^{-7} Torr. In each case, RDS spectra and RHEED patterns were measured at unison along the crystallographic direction [110]. In the RDS graphs presented for each experiment, spectra are vertically displaced and the zeros for each spectrum are indicated by horizontal black bars.

3.3.1 InAs/GaAs(001) growth at T=480°C and different As Overpressures

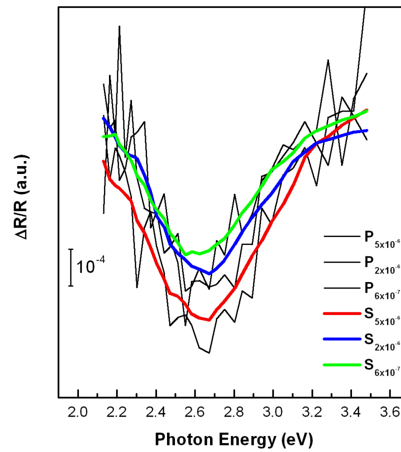

Figure 43: InAs/GaAs growth selected initial RD spectra and smoothings corresponding to growths at different As overpressure, $P_{As}=5x10^{-6}$Torr in red, $P_{As}=2x10^{-6}$Torr in blue and $P_{As}=6x10^{-7}$Torr in color green.

3.3.1.1 *Measurements along* [110] *and at* $P_{As}=5x10^{-6}$ *Torr*

With filled circles, in Fig.44a, are shown selected, time-resolved RD spectra acquired during the growth of InAs/GaAs QD's. Continuous lines in Fig.44a correspond to spectral fits; spectrum a) in Fig.44a was measured just before starting growth. It shows the typical line shape for a c(4x4) surface reconstruction with a minimum close to the GaAs E_1 interband energy transition [47]. Although this experiment was carried out at the same As overpressure as in the last 4 experiments, in comparison to its initial c(4x4) spectrum, this spectrum has somehow a greater broadness than the previous ones, so the interband energy transitions aren't as evident as in those first cases, but the general lineshape remains unchanged. This situation is originated, as was said before, due to the noise generated in the switching between the lock-in data-acquisition channel and the multiplexer. Spectra b)-e) were measured at various times during growth as indicated, with t=0 corresponding to growth onset. Spectrum f) was measured at the end of the experiment, with about 2 ML of InAs deposited on the GaAs substrate. In Fig.44b spectral components are shown though they are pretty robust too for the same reason explained before. But, the lineshapes of each spectral components are the same as the ones presented in previous analyses. The spectral components $Z_1(E)$ and $Z_2(E)$ are less sharp than any of the ones described in the previous section, but so are the spectra and its fits. The bump seen at high energies (around 2.9 eV) in Fig.44b at spectral component $Z_3(E)$, though seen also in the previous spectral components, in this case, it is enhanced, probably due to the noise in the spectra.

On the other hand, in Fig.45 is shown the contrast between the RHEED oscillation lineshape Fig.45b and the evolution in time of each of the spectral components posted in Fig.44b. The noise is also present in Fig.45a and it's seen in the red colored lineshape and its corresponding smoothings are shown in color black. The smoothings of these coefficients, $C_i(t)$ show the

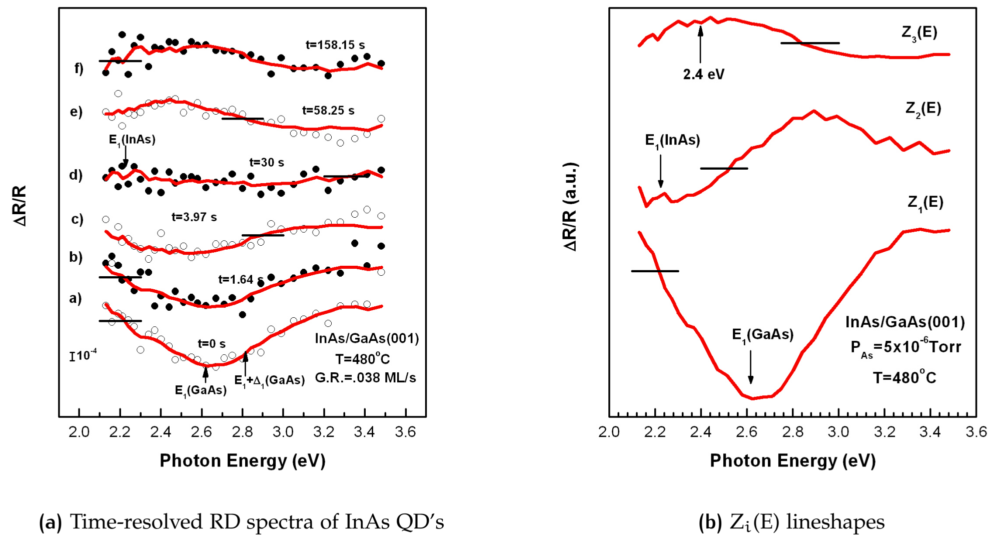

(a) Time-resolved RD spectra of InAs QD's

(b) $Z_i(E)$ lineshapes

Figure 44: InAs/GaAs growth selected time-resolved RD spectra and the $Z_i(E)$ lineshapes derived from an SVD analysis of such spectra.

same evolution that in the less noisy experiments. In the same way do the RHEED oscillations seen in Fig.45b, as it is expected in this first experiment, as the As overpressure and the substrate temperature are the same as in experiment in subsection 3.2.1.2. For this same reason, the RHEED diffraction patterns are being omitted in this set of experiments measured with the 2 channel lock-in.

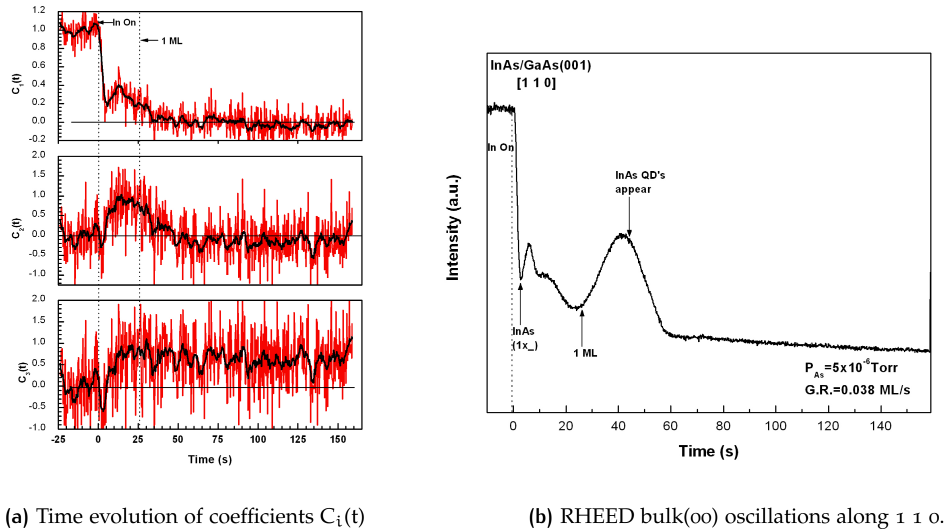

(a) Time evolution of coefficients $C_i(t)$

(b) RHEED bulk(00) oscillations along 1 1 0.

Figure 45: Time evolution of the three components (and its smoothings in black) that comprise the time-dependent RD spectra measured during the epitaxial growth of InAs/GaAs and RHEED oscillations of bulk(00) reconstruction lines along [110].

3.3.1.2 *Measurements along* [110] *and at* P_{As}= 2x10^{-6} *Torr*

In this particular experiment the As overpressure was that of P=2x10^{-6}Torr, the main change respect to the previously described experiment, comes in the comparison of the initial c(4x4) spectrum, the amplitude of this spectrum is smaller than the previous one as can be seen in Fig.43, but the general lineshape remains unchanged. This decrease in the amplitude of spectra (a) its due to the decrease in the As pressure (in respect to the previous experiments), as it can be related to the spectral evolution seen when a GaAs substrate is submitted to a change in temperature, passing from low temperatures to higher temperatures. In this kind of experiment, the GaAs spectrum seems to decrease in amplitude as the temperature starts increasing, this phenomena is also owed to the lack of As molecules in the GaAs surface as they tend to desorb at high temperatures. Though this decrease in amplitude, or in As molecules in the GaAs surface, doesn't seem to affect the adsorbing of In atoms, as it is described in the incoming anlysis. In Fig.46a spectra b)-e) were measured at various times during growth as indicated. Spectrum e) corresponds to that measured when 1 ML of InAs has been grown, though the significative noise during the measures, it can be appreciated that this spectrum has almost no structure, meaning that at this moment the anisotropies are almost null, it is observed that the spectrum is surrounding the zero black bar. This feature is also observed in spectra d) of Fig.44a. Spectrum f) was measured at the end of the experiment, with about 2 ML of InAs deposited on the GaAs substrate. Spectral components are shown in Fig.46b, the lineshapes of each spectral component are the same as the ones presented in the experiment with P=5x10^{-6}Torr As overpressure, with exception of the respectives bumps at high energies in the spectral components $Z_2(E)$ and $Z''_2(E)$.

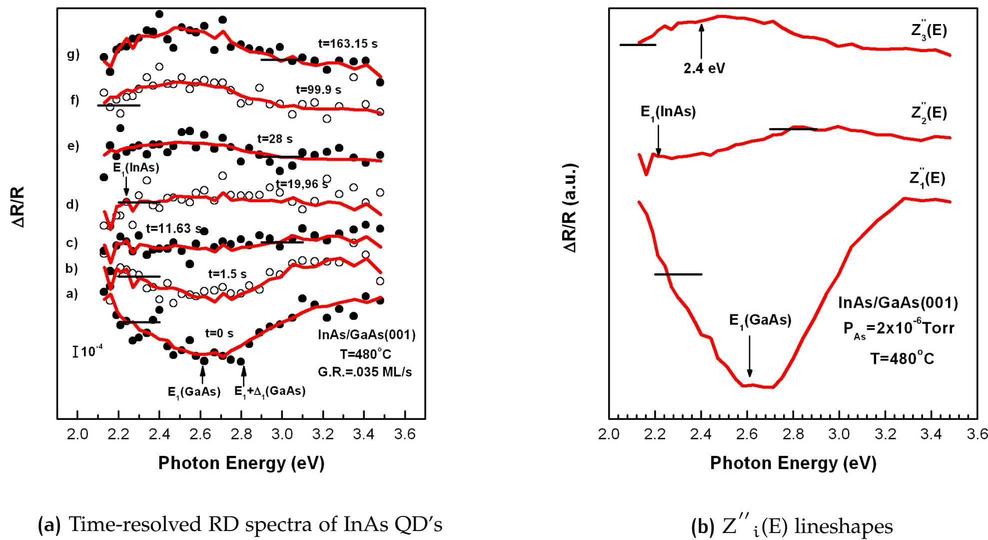

(a) Time-resolved RD spectra of InAs QD's

(b) $Z''_i(E)$ lineshapes

Figure 46: InAs/GaAs growth selected time-resolved RD spectra and the $Z''_i(E)$ lineshapes derived from an SVD analysis of such spectra.

In Fig.47a is shown the evolution in time of the corresponding spectral components, i.e. its coefficients $C''_i(t)$. It can be noticed that noise is still present during the measurement of this spectra, so a smoothing was necessary too, in fact, it seems that the lineshapes are noisier than the ones described in the previous subsubsection (3.3.1.1). On the other hand, RHEED oscillations seen in Fig.47b, show a noticeable difference in comparison to its analogous measured at P=$5x10^{-6}$Torr, the maximum where the QD's seem to appear, it's reduced to a small bump along the oscillation, though, the quantum dots are there, as they are registered by the RHEED diffraction patterns (not shown in this analysis). It is important to recall that the oscillations are those corresponding to the change of intensity of the bulk (00) diffraction spot. Being this important detail clarified, it is also pertinent to state that an observation made during the measurements of this experiments, was that in the cases where the As overpressure was lowered, the diffraction spots seen in the RHEED patterns where smaller (to the eye) than those measured at P=$5x10^{-6}$ Torr. Probably being this the reason the oscillations menguated its amplitude in this and the experiment that will be described in next section.

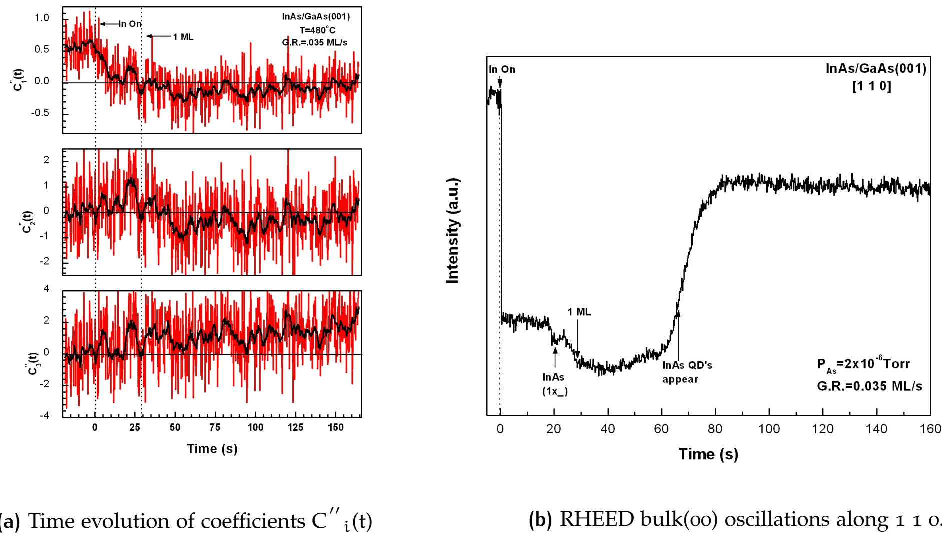

(a) Time evolution of coefficients $C''_i(t)$

(b) RHEED bulk(00) oscillations along 1 1 0.

Figure 47: Time evolution of the three components (and its smoothings in black) that comprise the time-dependent RD spectra measured during the epitaxial growth of InAs/GaAs and RHEED oscillations of bulk(00) reconstruction lines along [110].

3.3.1.3 *Measurements along* [110] *and at* P_{As}= $6x10^{-7}$ *Torr*

The As pressure during this growth was of P=$6x10^{-7}$ Torr, again the main change respect to the previously described experiments, comes in the comparison of the initial c(4x4) spectrum, the amplitude of this spectrum is smaller than the ones seen in Fig.43, but at the same time, it doesn't differ much from the amplitude of the spectrum measured at t=0 s in the experiment with As pressure of P=$6x10^{-7}$ Torr. In Fig.48a spectra b)-e) were measured at different times during growth. In Fig.48a there is no corresponding spectrum to that measured at 1 ML of InAs, or said in other words, measured when about 30 s had passed. But, observing spectrum b), which was measured after the growth of 1 ML of InAs, it is obvious that in this particular moment the GaAs structure is still detected by RDS as its characteristic structure is still seen in this spectrum. This might mean that as the growth rate is smaller than in the previous cases, when an entire monolayer InAs is supposed to be covering the surface, it is not, being partially covered by InAs and partially by GaAs, and probably being fully covered by InAs somewhere around (43-55) s time range. Spectrum f) was measured at the end of the experiment, with about 2 ML of InAs deposited on the GaAs substrate. Spectral components are shown in Fig.48b, the lineshapes of each spectral component are similar to those described in previous experiments.

Fig.49a shows the evolution in time of the corresponding spectral components and its respective smoothed lineshapes. The lineshapes have the same form as the ones in experiments in section 3.2, this attenuation of coefficient $C'''_1(t)$ around 45 s and the coexistance of coefficients $C'''_2(t)$ and $C'''_3(t)$ between 13 s and 40 s, which means that the InAs wetting layer described by $C'''_2(t)$ is still in its formation process while at unison, small quantum dots are being grown, see $C'''_3(t)$ at around 30s and its resemblance to its analogous coefficients at

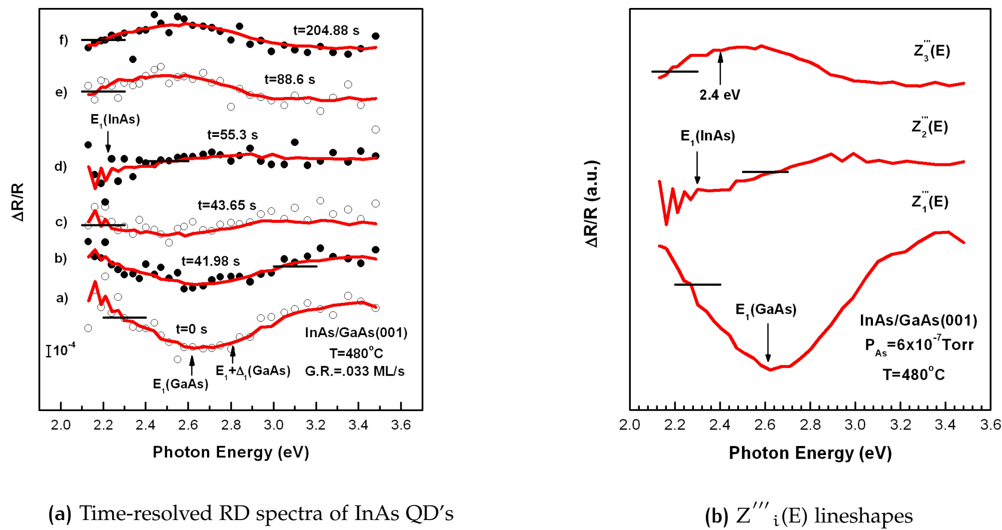

(a) Time-resolved RD spectra of InAs QD's

(b) $Z'''_i(E)$ lineshapes

Figure 48: InAs/GaAs growth selected time-resolved RD spectra and the $Z'''_i(E)$ lineshapes derived from an SVD analysis of such spectra.

section 3.2. As in experiments described before, RHEED oscillations seen in Fig.49b, show this noticeable difference in comparison to the one measured at P=5x10^{-6}Torr, as the maximum where the QD's seem to have appeared before, it is reduced to almost a null bump along the oscillation (see range between 45s and 65s), though, InAs quantum dots are there and appear to be smaller like in the experiment corresponding to an As overpressure of P=2x10^{-6} Torr. It is important to notice that this time range is almost the same as the one mentioned in the previous paragraph where due to RD spectra analysis that has been done, it can be refered to the probable moment where the surface is completely covered by InAs, though no necessarily in a layer by layer mode.

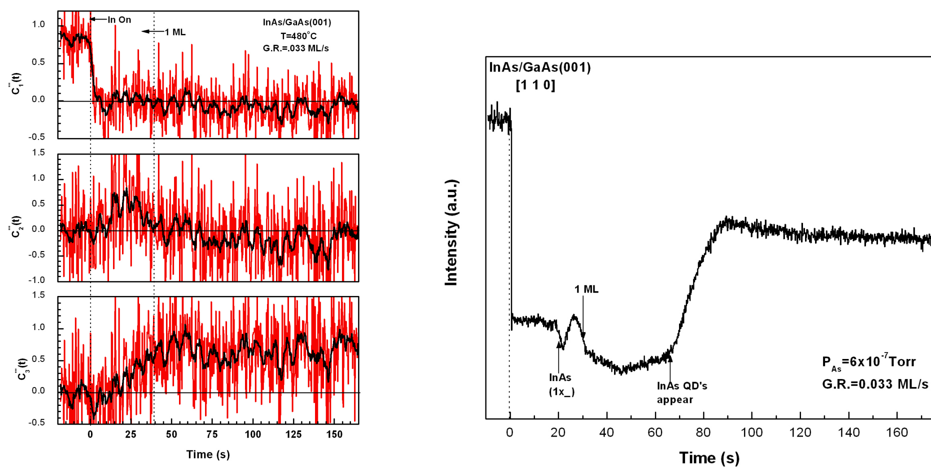

(a) Time evolution of coefficients $C'''_i(t)$

(b) RHEED bulk(00) oscillations along 1 1 0.

Figure 49: Time evolution of the three components (and its smoothings in black) that comprise the time-dependent RD spectra measured during the epitaxial growth of InAs/GaAs and RHEED oscillations of bulk(00) reconstruction lines along [110].

CONCLUSIONS

In the present work, the evolution of InAs grown by MBE on a GaAs(001)-c(4x4) surface was studied using two main characterization techniques, Real-Time RDS and RHEED as a complementary method. The research in this work detailed the evolutionary pathway during InAs growth in both regimes, 2D and its change to a 3D growth mode. The growth took place during two different growth conditions; 1) two different temperatures T_1=480°C and T_2=460°C under a constant As overpressure of P_{As}=5x10^{-6} Torr and 2) three different As overpressures P_1=5x10^{-6}Torr, P_2=2x10^{-6}Torr, P_3=6x10^{-7}Torr and a constant substrate temperature of T=480°C. In every case the same coverage evolution was observed (or inferred through a RDS analysis); the growth of InAs induced a change in the GaAs c(4x4) surface reconstruction turning it into an InAs (1x3) surface reconstruction in a really early stage during the growth (around the first 5 to 12 s during the diverse growth cases), this stage established the start of the InAs wetting layer formation, which was matched with an InAs small QDs unison growth, this can be corroborated looking at every experiment's $c_2(t)$ coefficient which start to fade after 1 ML of InAs was deposited. At this time, $c_3(t)$ starts to rise (in every single case), which represents the growth in size of the QDs, which are probable to be InGaAs QDs due to the transition energy (around 2.4 eV) seen in its spectral component $S_3(E)$. Such behavior is backgrounded with the STM analysis made by reference [5]. As mentioned also by [5] and as also being corroborated by the strain fits made during this study, strain is present along the whole growth, being in the same direction, due to the non-changing As dimmer direction (along the [110] crystallographic direction), until the WL is completely formated, after 1.4 ML, where the RD lineshape shows that the As dimmers had been rotated 90° (to the $[1\bar{1}0]$ crystallographic direction). While the formation of the InAs (2x4) surface, the rotation of the As dimmers is seen as well as is theoretically the formation of In dimmers along the [110] is also expected. At the same time, InGaAs QDs are shown in the same STM images and are also perceived by RD spectra at higher energies than those of pure InAs, whose corresponding critical point E_1 is 2.23 eV (at a temperature of T=480°C). This transition is seen in the $S_2(E)$ spectral component. Each of these features were also seen in the studies made by Jan Grabowski in [5], who used STM as characterization technique. This study is briefly described in Chapter 2, where the small InAs islands were observed at the same time as the GaAs c(4x4) surface was being covered with various InAs surface reconstructions. Again, references [24] and [25] are just some complementary examples of what can be inferred when InAs starts growing and how can it change the original GaAs c(4x4) surface reconstruction turning it into an InAs (1x3) surface reconstruction which represents the start of its wetting layer formation, at the same time that anistropies reduce [25] and start to increase again as InAs continues its deposition [24]. The study in reference [25] made by Takashi Kita et al., also makes reference to the saturation of kinetic RDS taken at 2.5 eV, this study denotes the triggering of InAs islands (see black arrows in Fig.11), phenomena reinforced by the present work where $c_3(t)$ in addition with its corresponding spectral components $S_3(E)$ and $c_2(t)$ and $S_2(E)$ comprehend the formation of small InAs QDs ($c_2(t)$) that eventually transform to bigger InGaAs QDs, which is marked out by the saturation of lineshape $c_3(t)$ and also suggested by different kind of studies made in reference

[5], as mentioned before.

Besides, in a rough mode, it seems like RHEED oscillations along [110] and with an As overpressure of P_{As}=5x10^{-6} Torr show similar features to those seen in c_2(t) and c_3(t). The InAs 1 ML deposition is seen at its maximum at both lineshapes c_2(t) and its corresponding measured RHEED oscillation. At the same time the c_3(t) lineshape saturation seems to be there too (at RHEED oscillations), but with an inverted sign, just before InAs QD's appear.

In summary:

The transition between two growth regimes, the 2D growth mode or layer by layer mode and the 3D growth mode was characterized by obtaining the evolution of the spectral components coefficients $c_i(t)$.

No matter which growth conditions were analyzed, 1) different temperatures with a constant As overpressure or 2) different As overpressures with a constant substrate temperature, the evolution of the spectral coefficients was the same.

Three spectral components comprise the formation of the measured experimental spectra. $S_1(E)$ corresponding to the c(4x4) GaAs surface reconstruction, $S_2(E)$ which represents the formation of small InAs QD's as a slight transition point is seen around 2.23 eV, on the other hand, $S_3(E)$ shows a higher transition energy at 2.4 eV and which correspond to the fully formatted InAs QD's. $S_3(E)$ has a similar lineshape as GaAs c(4x4) spectrum, but blue shifted and with an opposite sign.

$S_1(E)$ has the form of a well known line-shape, it corresponds to the strain (see reference [50] for its homoepitaxial analogous analysis) suffered by the GaAs subsurface due to the deposition of InAs' bigger atomic unit cell. $S_3(E)$ corresponds also to the strain release of the InAs deposited monolayers when it is recovering its unit cell size by the fully formed InGaAs QDs, this is concluded by the fact that the transition energy is seen around 2.4 eV which stands between GaAs and InAs critical points. $S_2(E)$ might represent the formation of small InAs QD's over a not fully formatted InAs wetting layer (partially formed by non-covered GaAs and partially by InAs).

The transformation of the GaAs c(4x4) surface reconstruction to an InAs (1x3) surface reconstruction during an early stage, stablished the wetting layer formation at the same time that small InAs QD's start to grow. Eventhough RHEED patterns do not make evident such small InAs QD's formation, RDS calculated spectral coefficients do show this feature when $c_2(t)$ starts to diminish its amplitude as $c_3(t)$ starts to gain an important weight.

In general terms, the results reported in this work demonstrate the potential for RD spectroscopy as an optical probe for the real-time monitoring of the epitaxial growth of InAs/GaAs QDs. We show that RD provides information on the kinetics of formation of QDs (in addition with complementary RHEED studies), including the rate of InAs coverage of the GaAs substrate, as well as the rate of growth of InGaAs QDs. Results further suggest that the formation

of QDs is mediated by the formation of small InAs-rich islands that eventually give place to bigger InGaAs QDs.

Appendices

A APPENDIX A

A.1 SINGULAR VALUE DECOMPOSITION

Singular value decomposition (SVD) can be looked at from three mutually compatible points of view. On the one hand, we can see it as a method for transforming correlated variables into a set of uncorrelated ones that better expose the various relationships among the original data items. At the same time, SVD is a method for idenifying and ordering the dimensions along which data points exhibit the most variation.This ties in to the third way of viewing SVD, which is that once we have identified where the most variation is, it's possible to find the best approximation of the original data points using fewer dimensions. Hence, SVD can be seen as a method for data reduction.

A.1.1 Example of Full Singular Value Decomposition

SVD is based on a theorem from linear algebra which says that a rectangular matrix A can be broken down into the product of three matrice, an orthogonal matrix U, a diagonal matrix S, and the transp ose of an orthogonal matrix V. The theorem is usually presented something like this:

$$A_{mn} = U_{mm}\Sigma_{mn}V_{nn}^{T} \tag{A.1}$$

where U^TU=I; V^TV=I; the columns of U are orthonormal eigenvectors of AA^T, the columns of V are orthonormal eigenvectors of A^TA, and Σ is a diagonal matrix containing the square roots of eigenvalues from U or V in descending order.

The following example merely applies this definition to a small matrix in order to compute its SVD. Lets start with the matrix:

$$A = \begin{bmatrix} 3 & 1 & 1 \\ -1 & 3 & 1 \end{bmatrix}$$

In order to find U, we have to start with AA^T. The transpose of A is

$$A^T = \begin{bmatrix} 3 & -1 \\ 1 & 3 \\ 1 & 1 \end{bmatrix}$$

so

$$AA^T = \begin{bmatrix} 3 & 1 & 1 \\ -1 & 3 & 1 \end{bmatrix} \begin{bmatrix} 3 & -1 \\ 1 & 3 \\ 1 & 1 \end{bmatrix} = \begin{bmatrix} 11 & 1 \\ 1 & 11 \end{bmatrix}$$

Next, we have to find the eigenvalues and corresponding eigenvectors of AA^T. We know that eigenvectors are defined by the equation $A\vec{v}=\lambda\vec{v}$, and applying this to AA^T gives us

$$\begin{bmatrix} 11 & 1 \\ 1 & 11 \end{bmatrix} \begin{bmatrix} x_1 \\ x_2 \end{bmatrix} = \lambda \begin{bmatrix} x_1 \\ x_2 \end{bmatrix}$$

We rewrite this as the set of equations

$$11x_1 + x_2 = \lambda x_1 \tag{A.2}$$

$$x_1 + 11x_2 = \lambda x_2 \tag{A.3}$$

and rearrange to get

$$(11 - \lambda)x_1 + x_2 = 0 \tag{A.4}$$

$$x_1 + (11 - \lambda)x_2 = 0 \tag{A.5}$$

Solve for λ by setting the determinant of the coeficient matrix to zero,

$$\begin{vmatrix} 11 - \lambda & 1 \\ 1 & 11 - \lambda \end{vmatrix} = 0$$

which works out as

$$\begin{aligned} (11 - \lambda)(11 - \lambda) - 1 \cdot 1 &= 0 \\ (\lambda - 10)(\lambda - 12) &= 0 \\ \lambda &= 10, \lambda = 12 \end{aligned} \tag{A.6}$$

to give us our two eigenvalues λ= 10; λ= 12. Plugging λ back in to the original equations gives us our eigenvectors. For λ= 10 we get

$$\begin{aligned} (11 - 10)x_1 + x_2 &= 0 \\ x_1 &= -x_2 \end{aligned} \tag{A.7}$$

which is true for lots of values, so we'll pick x_1= 1 and x_2=-1 since those are small and easier to work with. Thus, we have the eigenvector $[1, -1]$ correspondingto the eigenvalue λ= 10. For λ= 12 we have

$$\begin{aligned}(11-12)x_1 + x_2 &= 0 \\ x_1 &= x_2\end{aligned} \tag{A.8}$$

and for the same reason as before we'll take x_1= 1 and x_2=1. Now, for λ= 12 we have the eigenvector $[1, 1]$. These eigenvectors become column vectors in a matrix ordered by the size of the corresponding eigenvalue. In other words, the eigenvector of the largest eigenvalue is column one, the eigenvector of the next largest eigenvalue is column two, and so forth and so on until we have the eigenvector of the smallest eigenvalue as the last column of our matrix. In the matrix below, the eigenvector for λ= 12 is column one, and the eigenvector for λ=10 is column two.

$$\begin{bmatrix}1 & 1 \\ 1 & -1\end{bmatrix} = 0$$

Finally, we have to convert this matrix into an orthogonal matrix which we do by applying the Gram-Schmidt orthonormalization process to the column vectors. Begin by normalizing $\vec{v}_1$.

$$\begin{aligned}\vec{u}_1 = \frac{\vec{v}_1}{|\vec{v}_1|} = \frac{[1,1]}{\sqrt{1^2+1^2}} = \frac{[1,1]}{\sqrt{2}} = [\frac{1}{\sqrt{2}}, \frac{1}{\sqrt{2}}] \\ \vec{w}_2 = \vec{v}_2 - \vec{u}_1 \cdot \vec{v}_2 * \vec{u}_1 = \\ [1,-1] - [\frac{1}{\sqrt{2}}, \frac{1}{\sqrt{2}}] \cdot [1,-1] * [\frac{1}{\sqrt{2}}, \frac{1}{\sqrt{2}}] = \\ [1,-1] - 0 * [\frac{1}{\sqrt{2}}, \frac{1}{\sqrt{2}}] = [1,-1] - [0,0] = [1,-1]\end{aligned} \tag{A.9}$$

and normalize

$$\vec{u}_2 = \frac{\vec{w}_2}{|\vec{w}_2|} = [\frac{1}{\sqrt{2}}, \frac{-1}{\sqrt{2}}] \tag{A.10}$$

to give

$$U = \begin{bmatrix}\frac{1}{\sqrt{2}} & \frac{1}{\sqrt{2}} \\ \frac{1}{\sqrt{2}} & \frac{-1}{\sqrt{2}}\end{bmatrix} = 0$$

The calculation of V is similar. V is based on A^TA, so we have

$$A^TA = \begin{bmatrix}3 & -1 \\ 1 & 3 \\ 1 & 1\end{bmatrix}\begin{bmatrix}3 & 1 & 1 \\ -1 & 3 & 1\end{bmatrix} = \begin{bmatrix}10 & 0 & 2 \\ 0 & 10 & 4 \\ 2 & 4 & 2\end{bmatrix}$$

Find the eigenvalues of A^TA by

$$\begin{bmatrix} 10 & 0 & 2 \\ 0 & 10 & 4 \\ 2 & 4 & 2 \end{bmatrix} \begin{bmatrix} x_1 \\ x_2 \\ x_3 \end{bmatrix} = \lambda \begin{bmatrix} x_1 \\ x_2 \\ x_3 \end{bmatrix}$$

which represents the system of equations

$$\begin{aligned} 10x_1 + 2x_3 &= \lambda x_1 \\ 10x_2 + 4x_3 &= \lambda x_2 \\ 2x_1 + 4x_2 + 2x_3 &= \lambda x_3 \end{aligned} \tag{A.11}$$

which are rewritten as

$$\begin{aligned} (10-\lambda)x_1 + 2x_3 &= 0 \\ (10-\lambda)x_2 + 4x_3 &= 0 \\ 2x_1 + 4x_2 + (2-\lambda)x_3 &= 0 \end{aligned} \tag{A.12}$$

which are solved by setting

$$\begin{vmatrix} (10-\lambda) & 0 & 2 \\ 0 & (10-\lambda) & 4 \\ 2 & 4 & (2-\lambda) \end{vmatrix} = 0$$

This works out as

$$(10-\lambda)\begin{vmatrix} (10-\lambda) & 4 \\ 4 & (2-\lambda) \end{vmatrix} + 2\begin{vmatrix} 0 & (10-\lambda) \\ 2 & 4 \end{vmatrix} =$$

$$\begin{aligned} (10-\lambda)[(10-\lambda)(2-\lambda) - 16] + 2[0-(20-2\lambda)] &= \\ \lambda(\lambda-10)(\lambda-12) = 0, \end{aligned} \tag{A.13}$$

so λ= 0; λ= 10; λ= 12 are the eigenvalues for A^TA. Substituting λ back into the original equations to find corresponding eigenvectors yields for λ=12

$$\begin{aligned} (10-12)x_1 + 2x_3 = -2x_1 + 2x_3 &= 0 \\ x_1 &= 1, x_3 = 1 \\ (10-12)x_2 + 4x_3 = -2x_2 + 4x_3 &= 0 \\ x_2 &= 2x_3 \\ x_2 &= 2 \end{aligned} \tag{A.14}$$

So for λ= 12, $\vec{v}_1$= $[1, 2, 1]$. For λ= 10 we have

$$\begin{aligned}(10-10)x_1 + 2x_3 &= 2x_3 = 0\\ x_3 &= 0\\ 2x_1 + 4x_2 &= 0\\ x_1 &= -2x_2\\ x_1 &= 2, x_2 = -1\end{aligned} \tag{A.15}$$

which means for λ= 10, $\vec{v}_2$= $[2, -1, 0]$. For λ= 0 we have

$$\begin{aligned}10x_1 + 2x_3 &= 0\\ x_3 &= -5\\ 10x_1 - 20 &= 0\\ x_2 &= 2\\ 2x_1 + 8 - 10 &= 0\\ x_1 &= 1\end{aligned} \tag{A.16}$$

which means for λ= 0,$\vec{v}_3$= $[1, 2, -5]$. Order $\vec{v}_1$,$\vec{v}_2$, and $\vec{v}_3$ as column vectors in a matrix according to the size of the eigenvalue to get

$$\begin{bmatrix}1 & 2 & 1\\ 2 & -1 & 2\\ 1 & 0 & 5\end{bmatrix}$$

and use the Gram-Schmidt orthonormalization process to convert that to an orthonormal matrix.

$$\begin{aligned}\vec{u}_1 &= \frac{\vec{v}_1}{|\vec{v}_1|} = [\frac{1}{\sqrt{6}}, \frac{2}{\sqrt{6}}, \frac{1}{\sqrt{6}}]\\ \vec{w}_2 &= \vec{v}_2 - \vec{u}_1 \cdot \vec{v}_2 * \vec{u}_1 = [2, -1, 0]\\ \vec{u}_2 &= \frac{\vec{w}_2}{|\vec{w}_2|} = [\frac{2}{\sqrt{5}}, \frac{-1}{\sqrt{5}}, 0]\\ \vec{w}_3 = \vec{v}_3 - \vec{u}_1 \cdot \vec{v}_3 * \vec{u}_1 - \vec{u}_2 \cdot \vec{v}_3 * \vec{u}_2 &= [\frac{-2}{\sqrt{3}}, \frac{-4}{\sqrt{3}}, \frac{10}{\sqrt{3}}]\\ \vec{u}_3 &= \frac{\vec{w}_3}{|\vec{w}_3|} = [\frac{1}{\sqrt{30}}, \frac{2}{\sqrt{30}}, \frac{-5}{\sqrt{30}}]\end{aligned} \tag{A.17}$$

All this to give us

$$V = \begin{bmatrix}\frac{1}{\sqrt{6}} & \frac{2}{\sqrt{5}} & \frac{1}{\sqrt{30}}\\ \frac{2}{\sqrt{6}} & \frac{-1}{\sqrt{5}} & \frac{2}{\sqrt{30}}\\ \frac{1}{\sqrt{6}} & 0 & \frac{-5}{\sqrt{30}}\end{bmatrix}$$

what its really wanted is its transpose

$$V^T = \begin{bmatrix} \frac{1}{\sqrt{6}} & \frac{2}{\sqrt{6}} & \frac{1}{\sqrt{6}} \\ \frac{2}{\sqrt{5}} & \frac{-1}{\sqrt{5}} & 0 \\ \frac{1}{\sqrt{30}} & \frac{2}{\sqrt{30}} & \frac{-5}{\sqrt{30}} \end{bmatrix}$$

For S we take the square roots of the non-zero eigenvalues and populate the diagonal with them, putting the largest in s_{11}, the next largest in s_{22} and so on until the smallest value ends up in s_{mm}. The non-zero eigenvalues of U and V are always the same, so that's why it doesn't matter which one we take them from.Because we are doing full SVD, instead of reduced SVD, we have to add a zero column vector to S so that it is of the proper dimensions to allow multiplication between U and V. The diagonal entries in S are the singular values of A, the columns in U are called left singular vectors, and the columns in V are called right singular vectors.

$$S = \begin{bmatrix} \sqrt{12} & 0 & 0 \\ 0 & \sqrt{10} & 0 \end{bmatrix}$$

Now all the pieces of the puzzle are complete

$$A_{mn} = U_{mm} S_{mn} V^T_{nn} = \begin{bmatrix} \frac{1}{\sqrt{2}} & \frac{1}{\sqrt{2}} \\ \frac{1}{\sqrt{2}} & \frac{-1}{\sqrt{2}} \end{bmatrix} \begin{bmatrix} \sqrt{12} & 0 & 0 \\ 0 & \sqrt{10} & 0 \end{bmatrix} \begin{bmatrix} \frac{1}{\sqrt{6}} & \frac{2}{\sqrt{6}} & \frac{1}{\sqrt{6}} \\ \frac{2}{\sqrt{5}} & \frac{-1}{\sqrt{5}} & 0 \\ \frac{1}{\sqrt{30}} & \frac{2}{\sqrt{30}} & \frac{-5}{\sqrt{30}} \end{bmatrix} =$$

$$\begin{bmatrix} \frac{\sqrt{12}}{\sqrt{2}} & \frac{\sqrt{10}}{\sqrt{2}} & 0 \\ \frac{\sqrt{12}}{\sqrt{2}} & \frac{\sqrt{-10}}{\sqrt{2}} & 0 \end{bmatrix} \begin{bmatrix} \frac{1}{\sqrt{6}} & \frac{2}{\sqrt{6}} & \frac{1}{\sqrt{6}} \\ \frac{2}{\sqrt{5}} & \frac{-1}{\sqrt{5}} & 0 \\ \frac{1}{\sqrt{30}} & \frac{2}{\sqrt{30}} & \frac{-5}{\sqrt{30}} \end{bmatrix} = \begin{bmatrix} 3 & 1 & 1 \\ -1 & 3 & 1 \end{bmatrix}$$

These examples and explanation were taken from Kirk Baker Singular Decomposition Tutorial (reference [51]) due to its simplicity and clearness.

B APPENDIX B

B.1 SINGULAR VALUE DECOMPOSITION WOLFRAM MATHEMATICA CODE

Singular Value Decompo_Data6.nb

```
In[1]:= SetDirectory["/Users/April/Desktop/T8 InAs "];
        (*------------------------------------------------------------------------

        (*------------------------------------------------------------------------
        p1 = Import["pru8_31.txt", "Table"];

        pp11x = p1[[All, 1]];
        pp11y = p1[[All, 2]];
        n = Length[pp11x] / 31;
        Length[pp11x];

        (*For[s=1,s≤n,s+=2,
         pp11y[[32(s-1)+1;;32s]]=Reverse[pp11y[[32(s-1)+1;;32s]]];
         pp11x[[32(s-1)+1;;32s]]=Reverse[pp11x[[32(s-1)+1;;32s]]];
        ]*)

        Matrizexperimentos = {};

        For[i = 1, i ≤ n, i++,

         aux = {};
         For[j = 1, j ≤ 31, j++,
          experimento = pp11y[[j + 31 * (i - 1)]];
          AppendTo[aux, experimento]
         ];

         AppendTo[Matrizexperimentos, aux]
        ]

        Matrizexperimentos // MatrixForm;

        resultado = SingularValueDecomposition[Matrizexperimentos];

        Map[MatrixForm, %];

        valores = resultado[[1]].resultado[[2]].Transpose[resultado[[3]]];
        (* La reconstruccion de los vectores originales*)

        resultadobis = resultado[[2]].Transpose[resultado[[3]]] ;


        Finales = {};
        AppendTo[Finales,    Table[pp11x[[i]], {i, 1, 31}]    ];
```

Code Made by: Dr. Jorge Ortega from IICO

```
Singular Value Decompo_Data6.nb
Finales = {};
AppendTo[Finales,    Table[pp11x[[i]], {i, 1, 31}]   ];

For[i = 1, i ≤ n, i++,

 AppendTo[Finales, resultadobis[[ i]]   ]

]
FFinales = Transpose[Finales];
Export["ReSVD_pru831.txt", FFinales, "Table"];

Manipulate[
 experim = Table[pp11y[[j + 31 * (linea - 1)]], {j, 1, 31}];


 Show[

  ListPlot[(* resultadobis[[ linea]]*) valores[[linea]] , Joined → True, PlotRange → All,
   ColorFunction → Red], ListPlot[experim, PlotStyle → PointSize[0.04] ]
   ],

 {linea, 1, n, 1} ]
```

B.2 STRAIN MODEL WOLFRAM MATHEMATICA CODE

```
Exc.nb
SetDirectory[NotebookDirectory[]];
epsilon = Import["488DFGaAs.dat"];
LLλ = Import["Data58.dat"];
Base1 = Import["B1origin.dat"];
DerB1 = Import["Derivative1.dat"];

FD1 =.;
FD2 =.;
En =.;
A1 =.;
A2 =.;
Γ1 =.;
Γ2 =.;
Eg1 =.;
Eg2 =.;
θ1 =.;
θ2 =.;
dF1D1 =.;
dF2D2 =.;
dFD1 =.;
dFD2 =.;

(*Ajuste de Función Dieléctrica a F.D. de Literatura*)

epsimod = Table[0, {i, 1, 218}, {j, 1, 3}];

(*Constantes*)
D1 = 0.2; (*23*)

(*Forma de Línea 2D : E1*)

FD1 = (En^2) * (A1) * Exp[I * θ1] * (Eg1 - En - I * Γ1)^-1;
dFD1 = D[FD1, {En, 1}];
ddFD1 = D[dFD1, {En, 1}];
```

Code Made by: Abril Armenta from IICO

Exc.nb

```
(*Forma de Línea 2D : E1+D1*)

FD2 = (En^2) * (A2) * Exp[I * θ2] * (Eg2 - En - I * Γ2)^-1;
dFD2 = D[FD2, {En, 1}];
ddFD2 = D[dFD2, {En, 1}];

(*En^2 x las Funciones Dieléctricas*)

F1D1 = FD1;
dF1D1 = D[F1D1, {En, 1}];
F2D2 = FD2;
dF2D2 = D[F2D2, {En, 1}];

(*Parámetros E1*)

Eg1 = 2.615;
Γ1 = .225;
A1 = .25;
θ1 = (310) * (Pi / 180); (*-49, Eg1=2.6, Γ1=.24, A1=.26,LLλ[[i,1]]+0.06,
DRR[[i]]+0.021 ó 306, Eg1=2.6,Γ1=.225, A1=.25, LLλ[[i,1]]+0.028,DRR[[i]]+0.021,
ó 310, Eg1=2.615, Γ1=.23, A1=.25, LLλ[[i,1]]+0.019,DRR[[i]]+0.017, ó 305,
Eg1=2.615,Γ1=.225,A1=.24,LLλ[[i,1]]+0.012,DRR[[i]]+0.015, ó 309, Eg1=2.615,
Γ1=.22,A1=.24,LLλ[[i,1]]+0.016,DRR[[i]]+0.015*)

(*Parámetros E1+D1*)
Eg2 = Eg1 + D1;
Γ2 = .36;
A2 = .23;
θ2 = (310) * (Pi / 180); (*-49,Γ2=.32, A2=.22,X=.75*10^11, LLλ[[i,1]]+0.018,
dDRR[[i,1]]-.05 ó 306,Γ2=.34,A2=.22,X=.74*10^11, LLλ[[i,1]]+0.018,
dDRR[[i,1]]-.05 ó 310, Γ2=.36, A2=.23, X=.745*10^11, LLλ[[i,1]]+0.018,
dDRR[[i,1]]-.05 6305,Γ2=.34,A2=.22, X=.725*10^11, LLλ[[i,1]]+0.018,
dDRR[[i,1]]-.05 ó 309,Γ2=.34,A2=.22, X=.725*10^11, LLλ[[i,1]]+0.018,dDRR[[i,1]]-.05*)
```

Exc.nb

```
(*Ajuste de Funciones Dieléctricas*)
Do[En = LLλ[[i, 1]]; epsimod[[i, 1]] = LLλ[[i, 1]];
 epsimod[[i, 2]] = Re[ddFD1 + ddFD2] + 1 * -4 + 0 * 13;
 epsimod[[i, 3]] = Im[ddFD1 + ddFD2] + 1 * 2 + 0 * 6.9, {i, 1, 218}];


(*Gráficas Comparativas*)

(*Epsilon1*)
Graf1 = Table[{epsilon[[i, 1]], epsilon[[i, 6]]}, {i, 1, 218}];
Graf2 = Table[{epsimod[[i, 1]], epsimod[[i, 2]]}, {i, 1, 218}];
gp1 = ListPlot[{Graf1, Graf2}, PlotJoined -> True, PlotStyle → {Red, Blue},
  PlotStyle → Thick, PlotRange → All]


(*Epsilon2*)
Graf1 = Table[{epsilon[[i, 1]], epsilon[[i, 7]]}, {i, 1, 218}];
Graf2 = Table[{epsimod[[i, 1]], epsimod[[i, 3]]}, {i, 1, 218}];
gp1 = ListPlot[{Graf1, Graf2}, PlotJoined -> True, PlotStyle → {Orange, Green},
  PlotStyle → Thick, PlotRange → All]
```

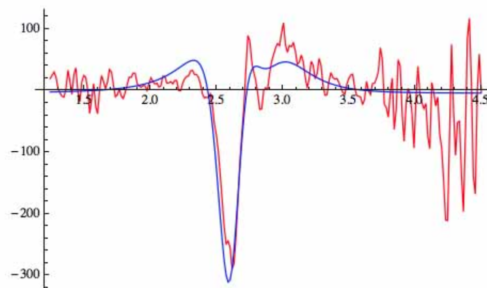

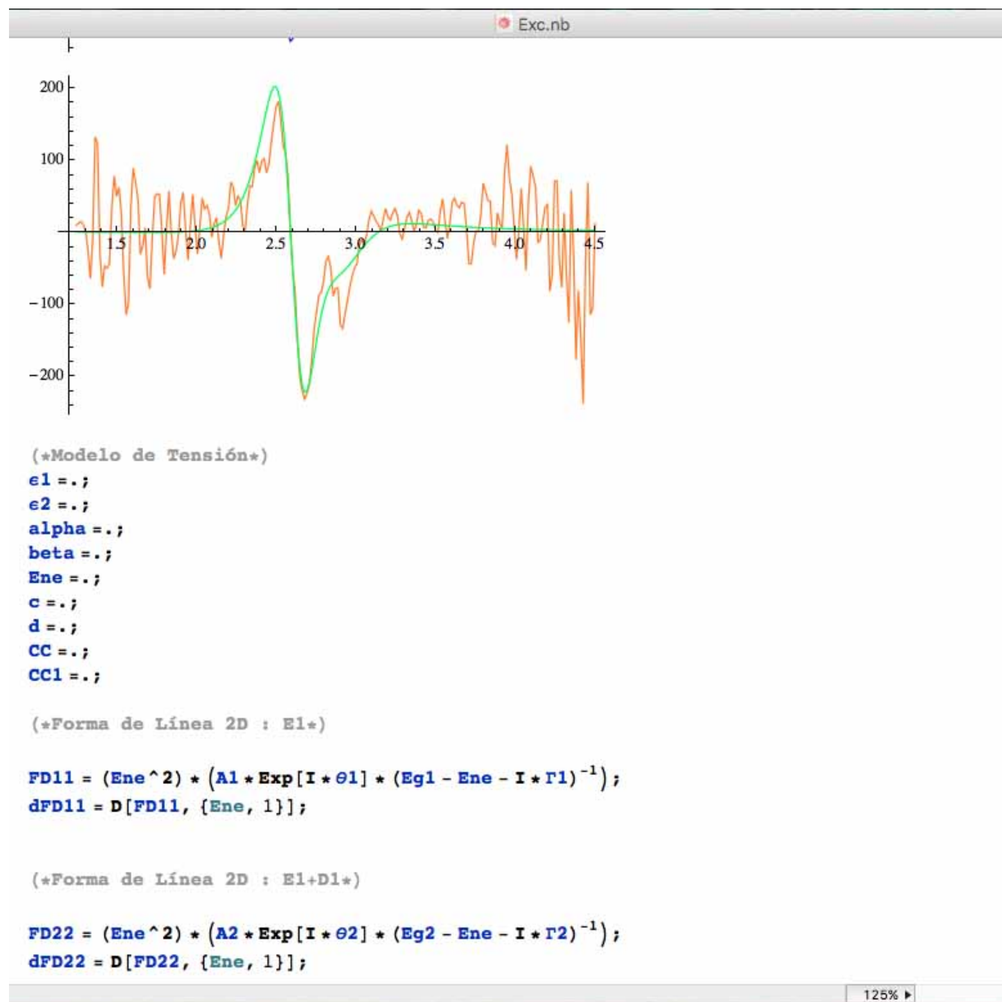

Exc.nb
200
100
-100
-200
1.5
2.0
2.5
3.0
3.5
4.0
4.5
(*Modelo de Tensión*)
ϵ1 =.;
ϵ2 =.;
alpha =.;
beta =.;
Ene =.;
c =.;
d =.;
CC =.;
CC1 =.;
(*Forma de Línea 2D : E1*)
FD11 = (Ene^2) * (A1 * Exp[I * θ1] * (Eg1 - Ene - I * Γ1)^-1);
dFD11 = D[FD11, {Ene, 1}];
(*Forma de Línea 2D : E1+D1*)
FD22 = (Ene^2) * (A2 * Exp[I * θ2] * (Eg2 - Ene - I * Γ2)^-1);
dFD22 = D[FD22, {Ene, 1}];
125%

Exc.nb

```
(*Forma de Línea 2D : E1+D1*)

FD22 = (Ene^2) * (A2 * Exp[I * θ2] * (Eg2 - Ene - I * Γ2)^-1);
dFD22 = D[FD22, {Ene, 1}];

CC = D[DD1/(Ene^2) * (dFD11 + dFD22) + DD2 * (FD11 - FD22), {Ene, 1}];

(*Coeficientes de Serafín*)

n = Sqrt[1/2 * (Sqrt[(ε1^2 + ε2^2)] + ε1)];
k = Sqrt[1/2 * (Sqrt[(ε1^2 + ε2^2)] - ε1)];
r = (1 - (n + I * k))/(1 + n + I * k);
(*R=r*Conjugate[r];*)
(*alpha=1/R *D[R,ε1] ;
beta=1/R *D[R,ε2];*)

alpha = (Sqrt[2] * (ε1^2 - ε2^2 - Sqrt[(ε1^2 + ε2^2)] + ε1 * (-1 + Sqrt[(ε1^2 + ε2^2)])))/
    (Sqrt[(ε1^2 + ε2^2)] * (1 - 2 * ε1 + ε1^2 + ε2^2) * (Sqrt[ε1 + Sqrt[(ε1^2 + ε2^2)]]));
beta = (Sqrt[2] * ε2 (-1 + 2 * ε1 + Sqrt[(ε1^2 + ε2^2)]))/
    (Sqrt[(ε1^2 + ε2^2)] * (1 - 2 * ε1 + ε1^2 + ε2^2) * (Sqrt[ε1 + Sqrt[(ε1^2 + ε2^2)]]));
```

125%

Exc.nb

```
alpha = (√2 * (ϵ1^2 - ϵ2^2 - √(ϵ1^2 + ϵ2^2)  + ϵ1 * (-1 + √(ϵ1^2 + ϵ2^2) )))/
    (√(ϵ1^2 + ϵ2^2) * (1 - 2 * ϵ1 + ϵ1^2 + ϵ2^2) * (√(ϵ1 + √(ϵ1^2 + ϵ2^2))));
beta = (√2 * ϵ2 (-1 + 2 * ϵ1 + √(ϵ1^2 + ϵ2^2)))/
    (√(ϵ1^2 + ϵ2^2) * (1 - 2 * ϵ1 + ϵ1^2 + ϵ2^2) * (√(ϵ1 + √(ϵ1^2 + ϵ2^2))));

CC1 = (alpha - I * beta) * CC;


ϵ1 = ϵpsilon[[All, 2]];
ϵ2 = ϵpsilon[[All, 3]];


(*Constantes2*)
X = .74 * 10^11; (*2.2x10^11*)
C11 = 11.88 * 10^11;
C12 = 5.38 * 10^11;
C44 = 5.94 * 10^11;
S11 = (C11 + C12) / ((C11 - C12) * (C11 + 2 * C12));
S12 = -C12 / ((C11 - C12) * (C11 + 2 * C12));
S44 = 1 / C44;
D11 = -8.40; (*-8.40+-0.8*) (*-7.26*)
D53 = -5; (*-6.40+-1.5*)
D51 = 8.8; (*9.20+-0.9*) (*7.75*)
dEh = D11 * (S11 + 2 * S12) * X / (Sqrt[3]);
DD2 = 2 * S44 * D53 * X / (D1 * (Sqrt[6]));
DD1 = D51 * S44 / (4 * Sqrt[3]) * X;

ΔFD = Table[0, {i, 1, 218}, {j, 1, 1}];
DRR = Table[0, {i, 1, 218}, {j, 1, 1}];
dDRR = Table[0, {i, 1, 218}, {j, 1, 1}];
Seraf1 = Table[0, {i, 1, 218}, {j, 1, 1}];
Seraf2 = Table[0, {i, 1, 218}, {j, 1, 1}];
```

125%

Exc.nb

```
Do[Ene = LLλ[[i, 1]];

 c = DD1/(Ene^2) * (dFD11 + dFD22);
 d = DD2 * (FD11 - FD22);

 ΔFD[[i]] = 1 * c + 1 * d;
 DRR[[i]] = Re[(alpha[[i]] - I * beta[[i]]) * ΔFD[[i]]]; Seraf1[[i]] = alpha[[i]];
 Seraf2[[i]] = beta[[i]]; dDRR[[i, 1]] = Re[CC1[[i]]], {i, 1, 218}]

(*Gráfica*)

Graf = Table[{LLλ[[i, 1]] + 0.016, DRR[[i]] + 0.019}, {i, 1, 218}];
ListPlot[{Graf, Base1}, PlotJoined -> True, PlotStyle → {Red, Blue}, PlotRange → All]
Export["AjusteExc2.dat", Graf];
Graf23 = Table[{LLλ[[i, 1]], Seraf1[[i]]}, {i, 1, 218}];
Graf24 = Table[{LLλ[[i, 1]], Seraf2[[i]]}, {i, 1, 218}];
Export["Alpha.dat", Graf23];
Export["Beta.dat", Graf24];
ListPlot[{Graf23, Graf24}, PlotJoined -> True, PlotStyle → {Red, Black}, PlotRange → All];


Graf25 = Table[{LLλ[[i, 1]] + 0.018, dDRR[[i, 1]] - .05}, {i, 1, 218}];
gp1 = ListPlot[{DerB1, Graf25}, PlotJoined -> True, PlotStyle → {Blue, Red},
  PlotStyle → Thick, PlotRange → All]
Export["AjDerivExc2.dat", Graf25];
```

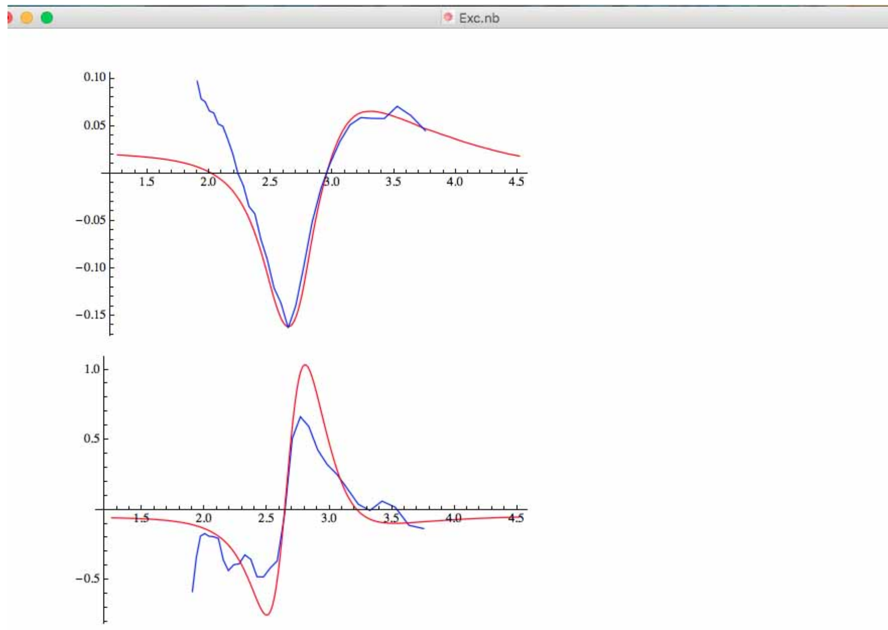
Exc.nb
0.10
0.05
−0.05
−0.10
−0.15
1.5
2.0
2.5
3.0
3.5
4.0
4.5
1.0
0.5
−0.5

BIBLIOGRAPHY

[1] Alfonso Lastras Martínez Viatcheslav A. Mischurnyi. *Láseres de Semiconductores*. Editorial Universitaria Potosina, 2010.

[2] Wolfgang Braun. *Applied RHEED, Reflection High.Energy Electron Diffraction During Crystal Growth*. Ed. by Karlsruhe Gerhard Höhler. Vol. 154. Germany: Springer-Verlag, 1999.

[3] Manuel Cardona Peter Y. Yu. *Fundamentals of Semiconductors (Physics and Materials Properties)*. Ed. by Professor William T. Rhodes Professor H. Eugene Stanley. Fourth Edition. Berlin: Springer-Verlag, 2010.

[4] Toh Ming Lu Gwo-Ching Wang. *RHEED Transmission Mode and Pole Figures: Thin Film and Nanostructure Texture Analysis*. New York: Springer, 2014.

[5] Jan Grabowski. "On the evolution of InAs thin films grown by molecular beam epitaxy on the GaAs(001) surface." PhD thesis. Technischen Universität Berlin, 2010.

[6] M. Ohring. *The Material Science of Thin Film*. New York: Academic Press, 1992.

[7] D.E. Aspnes. "Above-bandgap optical anisotropies in cubic semiconductores: A visible-ultraviolet probe surfaces." In: *J. Vac. Sci. Technol. B* 3 (1985), p. 1498.

[8] A. Maunder C.I. Smith P. Harrison T. Farrell and P. Weightman. "A rapid reflectance anisotropy spectrometer." In: *Meas. Sci. Technol.* 12 (2001), pp. 2185–2191.

[9] "A rapid reflectance-difference spectrometer for real-time semiconductor growth monitoring with sub-second time resolution." In: *Rev. Sci. Instrum.* 83 (2012), p. 103109.

[10] O. Núñez-Olvera R.E. Balderas-Navarro L.F. Lastras-Martínez L.E. Guevara-Macías D. Ariza-Flores J. Ortega-Gallegos and A. Lastras-Martínez. "A multichannel reflectance anisotropy spectrometer for epitaxial growth monitoring." In: *Meas. Sci. Technol.* 26 (2015), p. 115901.

[11] A.A. Studna D.E. Aspnes J.P. Harbison and L.T Florez. "Optical-reflectance and electron diffraction studies of molecular-beam epitaxy growth transients on GaAs (001)." In: *Phys. Rev. Lett.* 59 (1987), pp. 1687–90.

[12] D.E. Aspnes and A.A. Studna. "Anisotropies in the Above-Band-Gap Optical Spectra of Cubic Semiconductors." In: *Phys. Rev. Lett.* 54 (1985), p. 1956.

[13] D.E. Aspnes and A.A. Studna. "Low-retardance fused-quartz window for real-time optical applications in ultrahigh vacuum." In: *J. Vac. Sci. Technol. A* 7 (1989), p. 3291.

[14] 2016. URL: http://www.hindsinstruments.com/knowledge-center/technology-primer/pem-100photoelastic-modulation/principles-of-operation/.

[15] J.A. Venables. *Introduction to Surface and Thin Films Processes.* London: Cambridge University Press, 2000.

[16] A. Ichimiya and P.I. Cohen. *Reflection High-Energy Electron Diffraction*. London: Cambridge University Press, 2004.

[17] T. Hashizume Q.-K. Xue and T. Sakurai. "Scanning tunneling microscopy of III-V compound semiconductor (001) surfaces." In: *Prog. Surf. Sci.* 56 (1997), pp. 1–131.

[18] J.E. Northrup and S. Froyen. "Energetics of GaAs(100) (2x4) and (4x2) Reconstructions." In: *Phys. Rev. Lett.* 71 (1993), p. 2276.

[19] J.E. Northrup and S. Froyen. "Structure of GaAs(001) surfaces: The role of electrostatic interactions." In: *Phys. Rev. B.* 50 (1994), p. 2015.

[20] S. Tsukamoto N. Koguchi A. Ohtake J. Nakamura and A. Natori. "Structure Model for the GaAs(001) c(4x4) Surface." In: *Phys. Rev. Lett.* 89 (2002), p. 206102.

[21] "Kinetics in Surface Reconstructions on GaAs(001)." In: *Phys. Rev. Lett.* 92 (2004), p. 236105.

[22] S. Logothetidis P. Lautenschlager M. Garriga and M. Cardona. "Surface reconstructions on GaAs(001)." In: *Phys. Rev. B* 35 (1986), pp. 9174–9189.

[23] A. Ohtake. "Surface reconstructions on GaAs(001)." In: *Surf. Sci. Rep.* 63 (2008), pp. 295–327.

[24] T. Takagahara Y. Masumoto. *Semiconductor Quantum Dots: Physics, Spectroscopy and Applications.* Berlin: Springer-Verlag, 2002.

[25] T. Nakayama Takashi Kita Osamu Wada and M. Murayama. "Optical reflectance study of the wetting layers in (In,Ga)As self-assembled quantum dot growth on GaAs (001)." In: *Phys. Rev. B* 66 (2002), 195312–(1–6).

[26] D.M. Tex F. Yamada K. Shimomura T. Shirasaka and I. Kamiya. "RHEED transients during InAs quantum dot growth by MBE." In: *J. Vac. Sci. Technol. B* 30 (2012), 02B128–(1–4).

[27] A. Armenta-Franco and D. Ariza-Flores L.E. Guevara-Macías R.E. Balderas-Navarro L.F. Lastras-Martínez. A. Lastras-Martínez J. Ortega-Gallegos. "Real-time reflectance-difference spectroscopy during the epitaxial growth of InAs/GaAs(001)." In: *App. Surf. Sci.* Article in Press (2016).

[28] A. Lastras-Martínez K. Hingerl L F Lastras-L.F Lastras-Martínez R.E Balderas-Navarro. "Stress-induced optical anisotropies measured by modulated reflectance." In: *Semicond. Sci. Technol.* 19 (2004), R35–R46.

[29] R. E. Balderas-Navarro M. Chavira-Rodríguez A. Lastras-Martínez L. F. Lastras-Martínez J. M. Flores-Camacho. "Effect of reconstruction-induced strain on the reflectance difference spectroscopy of GaAs (001) around E1 and E1+ D1 transitions." In: *Phys. Rev. B* 75 (2007), 235315–(1–5).

[30] J. A. Appelbaum and D. R. Hamann. "Theory of reconstruction induced subsurface strain — application to Si(100)." In: *Surf. Sci.* 74 (1978), pp. 21–33.

[31] Tetsuji Yasuda Akihiro Ohtake Masashi Ozeki and Takashi Hanada. "Atomic structure of the GaAs(001)(24) surface under As flux." In: *Phys. Rev. B* 66 (2002), p. 209902.

[32] Masamitu Takahasi and Jun'ichiro Mizuki. "Element-Specific Surface X-Ray Diffraction Study of GaAs(001)c(44)." In: *Phys. Rev. Lett.* 96 (2006), p. 055506.

[33] S. Logothetidis P. Lautenschlager M. Garriga and M. Cardona. "Interband critical points of GaAs and their temperature dependence." In: *Phys. Rev. B* 35.9174-9189 (1987).

[34] Manuel Cardona and Gunter Harbeke. "Excitons at the L Absorption Edge in Zinc Blende-Type Semiconductors." In: *Phys. Rev. Lett.* 8 (1962), p. 90.

[35] R. E. Balderas-Navarro-J. M. Flores-Camacho M. E. Chavira-Rodríguez A. Lastras-Martínez L. F. Lastras-Martínez J. Ortega-Gallegos and M. Cardona. "Surface strain contributions to the lineshapes of reflectance difference spectra for one-electron and discrete-exciton transitions." In: *phys. stat. sol. (c)* 5.8 (2008), pp. 2591 –2594.

[36] L.E. Guevara-Macías O. Núñez-Olvera R.E. Balderas-Navarro L.F. Lastras-Martínez-L.A. Lastras-Montaño A. Lastras-Martínez J. Ortega-Gallegos and M.A. Lastras-Montaño. "Real-time reflectance-difference spectroscopy of GaAs molecular beam epitaxy homoepitaxial growth." In: *Appl. Phys. Lett. Matter.* 2 (2014), p. 032107.

[37] D.E. Aspnes U. Rossow L. Mantese. "Lineshapes of surface induced optical anisotropy spectra measured by RDS/RAS." In: *App. Surf. Sci.* 123/124 (1998), pp. 237–242.

[38] R. E. Balderas-Navarro-J. M. Flores-Camacho L. F. Lastras-Martínez M. Chavira-Rodríguez and A. Lastras-Martínez. "Reflectance difference spectroscopy of GaAs (001) under a [110] uniaxial stress." In: *Phys. Rev. B* 70 (2004), 035306–(1–7).

[39] Y. Girard-A. Coati Y. Garreau-M. Hohage L. D. Sun G. Prévot B. Croset and P. Zeppenfeld. "Elastic origin of the O/Cu(1 1 0) self-ordering evidenced by GIXD." In: *Surf. Sci.* 549 (2004), p. 52.

[40] L. F. Lastras Martínez and A. Lastras-Martínez. "Reflectance anisotropy of GaAs(100): Dislocation-induced piezo-optic effects." In: *Phys. Rev. B* 54 (1996), p. 10726.

[41] D. E. Aspnes and A. A. Studna. "High Precision Scanning Ellipsometer." In: *Appl. Opt* 14 (1975), pp. 220–228.

[42] E. Placidi-P. Chiaradia M. Fanfoni-F. Patella C. Hogan F. Arciprete C. Goletti and A. Balzarotti. "Surface versus bulk contributions from reflectance anisotropy and electron energy loss spectra of the GaAs(001)c(44) surface." In: *Phys. Rev. B* 68 (2003), p. 125328.

[43] A. A. Studna L. T. Florez H. H. Farrell D. E. Aspnes Y. C. Chang and J. P. Harbison. "Direct optical measurement of surface dielectric responses: Interrupted growth on (001) GaAs." In: *Phys. Rev. Lett.* 64 (1990), p. 192.

[44] F. Fleischer C. Cobet N. Esser W. Richter J. Bernholc W. G. Schmidt F. Bechstedt and G. Onida. "GaAs(001): Surface Structure and Optical Properties." In: *phys. stat. sol. (a)* 188 (2001), pp. 1401–1409.

[45] N.N. Ledentsov D. Bimberg M. Grundmann. *Quantum Dot Heterostructures*. New York: Wiley, 1998.

[46] M. Grundmann. *The Physics of Semiconductors*. Berlin, Heidelberg: Springer-Verlag, 2010.

[47] L.T Florez I. Kamiya D.E. Aspnes and J.P. Harbison. "Reflectance difference spectroscopy of GaAs (001) surfaces in ultra high vacuum." In: *Phys. Rev. B* 46 (1992), pp. 15894–15904.

[48] Y.J. Park Hosun Lee S.M. Kim and E.K. Kim. "Ellipsometric study of InAs wetting layer in InAs/GaAs quantum dots at the threshold of quantum dot formation." In: *J. Appl. Phys.* 90 (2001), pp. 2290–2295.

[49] D. Esposito L. Grazulis M. Hill K. Mahalingam K.G. Eyink F. Szmulowicz and A.J. Aronow. "Evaluation of thickness and strain of thin planar layers of InAs on GaAs (001) using spectroscopic ellipsometry." In: *Appl. Phys. Lett* 105 (2014), p. 031909.

[50] L.E. Guevara-Macías O. Núñez-Olvera R.E. Balderas-Navarro L.F. Lastras-Martínez-L.A. Lastras-Montaño A. Lastras-Martínez J. Ortega-Gallegos and M.A. Lastras-Montaño. "Reflectance-difference spectroscopy as a probe for semiconductor epitaxial growth monitoring." In: *J. Cryst. Growth* 1 (2015), pp. 1–4.

[51] 2017. URL: https://davetang.org/file/Singular_Value_Decomposition_Tutorial.pdf.

[52] K. Kuhler P. Ganser-W. Rothemund P. Hiesinger T. Schweizer and W. Jant. "Anisotropic electrical conduction in $GaAs/In_{0.2}Ga_{0.8}As/Al_{0.3}Ga_{0.7}As$ strained heterostructures beyond the critical layer thickness." In: *J. Appl. Phys.* 72 (1992), pp. 2941–2946.

[53] A.A. Saranin A.V. Zotov K. Oura V.G. Lifshits and M. Katayama. *Surface Science: An Introduction*. Berlin: Springer-Verlag, 2003.

[54] 2016. URL: http://andrew.gibiansky.com/blog/mathematics/cool-linear-algebra-singular-value-decomposition/.

[55] E.F. Schubert. *Delta-doping of semiconductors*. New York: Cambridge University Press, 1996.